

Numerical Simulation of Two-Phase Turbulent Flows in Ash Circulating Fluidized Bed

IGOR KRUPENSKI

Faculty of Mechanical Engineering
Department of Thermal Engineering
TALLINN UNIVERSITY OF TECHNOLOGY

Dissertation was accepted for the defence of the degree of Doctor of Philosophy in Engineering on April 23, 2010

Supervisors:

Prof. Ph D Andres Siirde, Faculty of Mechanical Engineering

D Sc Alexander Kartushinsky, Faculty of Science

Opponents:

Prof. D Sc Aleksandr Schreiber, Institute of General Energy, Ukrainian Academy of Sciences, Head of the Systems Analysis and Prognostication of R&D Progress in Power Sector

Ph D Aleksandr Schmidt, Head of the Computational Physics Laboratory, Ioffe Physical Technical Institute, Russian Academy of Sciences

Defence of the thesis: May 21, 2010, 11:00

Lecture hall V-215

Tallinn University of Technology, Ehitajate tee 5, Tallinn

Declaration

Hereby I declare that this doctoral thesis, my original investigation and achievement, submitted for the doctoral degree at Tallinn University of Technology has not been submitted for any academic degree.

Copyright: Igor Krupenski, 2010

ISSN 1406-4758

ISBN 978-9985-59-892-4

MASINA- JA APARAADIEHITUS E50

**Turbulentsete kahefaasiliste voolude
matemaatiline modelleerimine
tuha tsirkuleerivas keevkihis**

IGOR KRUPENSKI

CONTENTS

INTRODUCTION.....	7
NOMENCLATURE.....	10
1 THEORETICAL PART OF CIRCULATING FLUIDIZED BED	
HYDRODYNAMICS.....	15
1.1 Short introduction of Circulating Fluidized Bed.....	15
1.1.1 Boiler heating surface fouling.....	19
1.1.2 Oil-Shale ash properties.....	20
1.2 Fluidized beds and fluidization.....	22
1.3 Overview of existing mathematical models.....	22
1.3.1 Models.....	22
1.3.2 Mass conservation.....	23
1.3.3 Turbulence.....	23
1.3.4 Drag viscous force.....	27
1.3.5 Lift forces.....	30
1.3.6 Buoyant force.....	30
1.3.7 Particle-particle and particle-wall interactions.....	31
1.4 Purposed solution.....	33
2 TURBULENT BOUNDARY LAYER AND TWO-DIMENSIONAL	
REYNOLDS AVERAGED NAVIER-STOKES MODELING.....	34
2.1 Main predictions.....	34
2.1.1 Turbulent Boundary Layer.....	34
2.1.2 2-Dimensional Reynolds Averaged Navier-Stokes.....	34
2.2 Governing equations.....	35
2.2.1 Turbulent Boundary Layer equations.....	35
2.2.2 2-Dimensional Reynolds Averaged Navier-Stokes equations.....	36
3 MODEL APPLICATIONS.....	40
3.1 Numerical simulation.....	40
3.2 Numerical modeling for circulating fluidized bed conditions.....	46
4 RESULTS AND DISCUSSIONS.....	49
4.1 Turbulent Bondary Layer modeling.....	49
4.2 2-Dimensional Reynolds Averaged Navier-Stokes modeling.....	54
CONCLUSIONS.....	63
REFERENCES.....	64
LIST OF PUBLICATIONS.....	69

KOKKUVÕTE.....	70
ABSTRACT	71
CURRICULUM VITAE	72
ELULOOKIRJELDUS.....	73

INTRODUCTION

Motivation of the study

Fluidized beds are units designed to achieve fluid-solid contacting by the flow of fluid through a bed of particles [2]. Many thermal processes in industry take advantage of the significant fluid-solid contacting in fluidized beds to carry out fluid-solid reactions, heterogeneous catalysis and particle drying. Gas-solid fluidization process in circulating fluidized beds is widely applied in many industries. Characterization of gas-particle two-phase flow in a circulating fluidized bed (CFB) riser is important for process optimization. The particle size distribution has a significant influence on the gas-solid flow dynamics [20].

Gas-fluidized beds consist of fine granular material that are subject to a gas flow from below, large enough so that the gas drag on the particles can overcome the gravity and the particles can fluidize. When in the fluidized state, the moving particles work effectively as a mixer resulting in a uniform temperature distribution and a high mass transfer rate, which are beneficial for the efficiency of many physical and chemical processes [71]. For this reason, gas-fluidized beds are widely applied in different industries: thermal, energy, chemical, petrochemical, metallurgical, and environmental industries in large-scale operations involving adhesion optimized coating, granulation, drying, and synthesis of fuels and base chemicals (Kunii and Levenspiel, 1991). Lack of understanding of the fundamentals of dense gas-particle flows in general has led to severe difficulties in the design and scale-up of these industrially important gas-solid contactors (van Swaaij, 1985). In most cases, the design and scale-up of fluidized bed reactors is a fully empirical process based on preliminary tests on pilot-scale model reactors, which is a very time consuming and thus expensive activity. Clearly, computer simulations can be a very useful tool to aid this design and scale-up process.

Concentration of solid particles of the ash and inert material taken place in a combustion chamber of the circulating fluidized bed is very high, that gives a rise to some disadvantages. At the same time, the required temperature level occurred in a combustion chamber is guaranteed by the circulation of solid particles. In accordance with a widespread introduction of the CFB furnaces in power plants the concentration of the ash solid particles in the furnace gases substantially increases. The ash particles of the pulverised firing boilers can be observed in the furnace gases as an inconvenient admixture. These particles pose specific problems such as the behaviour of inorganic matter in combustion process, fouling, high temperature corrosion and wear of the steam boilers heating surfaces. In the CFB furnaces the ash solid particles are used mainly as the solid heat carrier – separated in hot cyclone and cooled in heat exchange the ash particles come back into the furnace. By the circulating ash mass the temperature level in furnace is held in the given range. While the heat capacity of ash is quite low, then the circulating ash mass must be high. The high ash concentration in furnace gases is attained a) by the high velocity of gas in the bed and that of most fuel particles carried out of bed are burned and their ash fills the whole volume of furnace

and b) by the ash circulation. The CFB combustion technology enables to bind the sulfur components with the carbonate components added to the fuel or existing within the mineral part of the fuel.

A disadvantage of CFB is that some fuel ash particles become too fine during the circulation and therefore the size of the ash particles contained in the fuel gas exiting the hot cyclone is too small. As a result of disintegration, the mass of the fine ash particles, which are not separated from the flue gases or occurred in the connective flue ducts and in the multicyclone, increases. The high concentration of particles in the fire gases of the CFB furnace chamber contributes to the formation of the particle clusters with the solid phase concentration within $0.1 - 0.2 \text{ m}^3/\text{m}^3$. At the exit of the CFB boiler furnace the density of solid phase is within $5 - 20 \text{ kg}/\text{m}^3$.

Objectives of the thesis

Objectives of the thesis are:

- Overview of existing mathematical models for CFB modeling
- Turbulent Boundary Layer (TBL) and 2-Dimensional Reynolds Averaged Navier-Stokes (2D RANS) models
- Gas-particle turbulent flow numerical simulation
- Practical initial data, using the characteristics of Estonian oil-shale ash

Approval of the results

The results of this work were presented at proceedings:

- The 6th International Symposium „Topical Problems in the Field of Electrical and Power Engineering“. Doctoral School of Energy and Geotechnology. Kuressaare, Estonia, January 12-17, 2009.
- The 7th International Symposium „Topical Problems in the Field of Electrical and Power Engineering“. Doctoral School of Energy and Geotechnology. Pärnu, Estonia, January 11-16, 2010.
- 7th International Conference of Young Scientists on Energy Issues „CYSENI 2010“. Kaunas, Lithuania, May 27-28, 2010 (accepted for participation)

Scientific novelty of the thesis

The scientific novelty of the thesis is a gas-solid particle turbulent flow numerical simulation, taking in the advance the real initial data of CFB power plants using Estonian oil-shale ash.

There was composed a mathematical model which simulates CFB riser. The results of the simulation describe the behaviour of oil-shale ash particles in CFB, which could be helpful in improving the efficiency of the combustion process.

The possibility of proceeding the research is to use the mixture of oil-shale ash and sand as the solid phase of the flow.

Acknowledgements

I would like to express my gratitude to everyone who has in one way or another contributed to this work. The author would like to express his deepest gratitude to his supervisors, Prof. Ph D A.Siirde and D Sc A.Kartushinsky, for their excellent guidance and support during this research. I would like to thank my family, friends and my bride Yulia for constant support, understanding and encouragement at different stages of the present work. I dedicate this work to my farther, mathematician Aleksei Krupenski.

NOMENCLATURE

Roman symbols

A	-	representative area of the droplet
C	-	mass concentration of the dispersed phase, [kg/m ²]
C'_D	-	factor of drag coefficient
C_D	-	drag coefficient
C_M	-	coefficient of Magnus force
C_ω	-	coefficient of torque
C_1-C_3	-	numerical constants for torque
f	-	drag factor corrected to multiple particle effects
f_c	-	frequency of particulate collision
\bar{F}	-	force
F_B	-	buoyant force, [1/s]
F_s	-	Saffman force, [1/s]
F_D	-	drag force, [1/s]
F_{faxen}	-	Faxen force, [1/s]
F_{Stokes}	-	Stokes force, [1/s]
Fr	-	Froude number
d	-	diameter of particle, [m]
d_i	-	diameter of colliding particle, [m]
d_j	-	diameter of colliding particle, [m]
D	-	pipe diameter, [m]
D_p	-	particle diameter, [m]
D_s	-	coefficient of diffusion, [m ² /s]
D_{ci}	-	diffusion coefficient of particles, [m ² /s]
E_d	-	energy added per unit mass to the flow
g	-	gravitation acceleration, [m/s ²]
k	-	turbulent energy, [m ² /s ²]
k_i	-	turbulent energy in the flow without particles, [m ² /s ²]
k_n	-	particle restitution coefficient
k_s	-	energy of dispersed phase from particle collision, [m ² /s ²]
l	-	characteristic length, [m]
L	-	integral turbulence length scale, [m]
L_e	-	length scale characteristic of the most energetic turbulent eddies, [m]
L_i	-	dissipation length scale in the flow without particles, [m]

L_h	-	“hybrid“ length scale, [m]
\dot{m}_k	-	mass rate
nm^3	-	unit volume at normal conditions, [nm ³]
n_{ij}	-	concentration of the group of particles „j“, which may collide with the group of particles „i“
p	-	pressure, [kg/ms ²]
P	-	turbulence modulation
P_d	-	production due to particles
P_i	-	inherent production
r	-	radial coordinate, [m]
R	-	pipe radius, [m]
Re	-	Reynolds number
Re_p	-	particle Reynolds number
Re_r	-	Reynolds number based on the relative velocity
S_{mass}	-	mass source term per unit volume
St	-	Stokes number
t_c	-	time scale of interparticle collision
T	-	the temperature of the flow, [°C]
T_*	-	characteristic time of hydrodynamic process, [s]
q_k	-	part of heat, separated from furnace with sensible heat of fly ash, [%]
Q_i^r	-	fuel calorific value as it used, [MJ/kg]
u	-	axial velocity component, [m/s]
u_i	-	mass average velocity, [m/s]
u_j^i	-	axial velocity at grid points (i, j) , [m/s]
u_l	-	velocity of the continuous phase, [m/s]
\bar{u}	-	gas velocity over cross-section, [m/s]
\tilde{u}	-	total axial velocity including drift turn, $\tilde{u} = u - D_s \frac{\partial \alpha}{\partial x}$, [m/s]
v	-	radial velocity component, [m/s]
v_j^i	-	radial velocity at grid points (i, j) , [m/s]
v_l	-	velocity of the particle, [m/s]
v_*	-	friction velocity of gas, [m/s]
\bar{v}	-	radial velocity over cross-section, [m/s]
\tilde{v}	-	total radial velocity including drift turn, $\tilde{v} = v - D_s \frac{\partial \alpha}{\partial y}$, [m/s]

V	-	unit volume
\vec{V}	-	velocity vector
V_o	-	theoretical amount of air for combustion of one kg fuel, [nm^3/kg]
V_g	-	amount of fire gases raised during combustion of one kg fuel, [nm^3/kg]
V_i	-	velocity of colliding particle, [m/s]
V_j	-	velocity of colliding particle, [m/s]
x	-	axial coordinate, [m]
x_i	-	axial coordinate, [m]

Greek symbols

α	-	particle mass concentration
α_c	-	volume fraction of the continuous phase
β	-	corresponding mass loading
δ	-	particle diameter, [m]
Σ	-	summation over all particle fractions
ε	-	dissipation rate of turbulent energy, [m^2/s^3]
ε_d	-	dissipation due to particles, [m^2/s^3]
ε_h	-	rate of dissipation of the turbulent energy of the gaseous phase, [m^2/s^3]
Σ	-	summation over all particle fractions
η	-	boiler efficiency, [%]
η_c	-	cyclone ash separation efficiency, [%]
ρ	-	density of gas, [kg/m^3]
ρ_d	-	dispersed phase density, [kg/m^3]
ρ_c	-	density of the continuous (conveying) phase, [kg/m^3]
ρ_p	-	density of gas and material of particles, [kg/m^3]
τ	-	response time, [s]
τ_i	-	response time for the “i” fraction of particles, [s]
τ_p	-	particle response time, [s]
τ_V	-	response time for the Stokes regime, [s]
σ	-	turbulent energy for two-phase flow, [m^2/s^2]
σ_0	-	turbulent energy for single-phase flow, [m^2/s^2]
Ω	-	angular velocity slip between gas- and dispersed phases, [1/s]
μ	-	dynamic viscosity, [kg/ms]

$\bar{\mu}$	-	ratio of the viscosity of the carrier phase to that of the fluid sphere
ν	-	kinematic viscosity, [m ² /s]
ω	-	angular velocity, [1/s]
∇^2	-	evaluated at the position of the particle
Δ	-	numerical step grid
$\Delta c = c_{ls} - c_{lv}$	-	difference of sensible heat of separated hot and cooled fly ashes, [MJ/kg _{ash}]
$\Delta x, \Delta r$	-	numerical mesh sizes
γ	-	specific weight of the fluid
λ	-	inter-particle spacing, [m]
\forall	-	volme of the body

Subscripts

c	-	continuous phase
i	-	i-th particle fraction of dispersed phase
g	-	gas
g_i, g_j, g_k	-	different gas phases
k	-	droplet/particle
N	-	number of droplets in the control volume plus the pairs of complementary droplets on the boundary
p	-	particle property
s_i	-	i-th fraction of dispersed phase
t	-	turbulent
θ	-	parameters of single-phase flow & dynamic friction
'	-	fluctuation & post-collision
ω	-	rotation

Superscripts

xx	-	axial component
rr	-	radial component
xr	-	cross-correlation component
x ω	-	axial-angular component
r ω	-	radial-angular component
ω	-	angular component

1 THEORETICAL PART OF CIRCULATING FLUIDIZED BED HYDRODYNAMICS

1.1 Short introduction of Circulating Fluidized Bed

Over 90% of electricity produced in Estonia is made by power plants firing local oil-shale and 25% of the boilers are of the circulating fluidized bed (CFB) variety [1]. Combusting solid fuels by fluidized bed is quite a new method in thermal power stations. There are known three technologies of fluidized bed [53]:

- Classical fluidized bed
- Circulating fluidized bed
- Excess pressure fluidized bed

Fluidized bed is the fine solid particles hovering system in gas flows, which inside motion gives it fluid properties, so arises pseudo-fluid and that is how fluidized bed is called. Solid particles layer becomes a fluidized bed layer in a gravitation field if the blown particles gas flow dynamic pressure force equilibrates the gravity force of the particles. If we append the fine fuel to bed of the solid particles, which temperature at least equals the fire point of the fuel, then there will be a continuous combustion and no high temperature would be needed. That is the reason why the fuel fluidized bed combustion belong to the category of the low-temperature combustion technology.

In the case of the fuel with the small mineral part, sand is oftenly used as a material of the fluidized bed. Oil-shale is a fuel with a big mineral part, so there is no need of sand and the material, used for the fluidized bed, is ash, which is formed in combustion process. The originality of the circulating fluidized bed process is that two-phase flow (gas and solid particles), outgoing from furnace, heads to the separator where the bigger ones (by mass and size) particles (in case of oil shale they are ash particles) are separated and guided back to the furnace. In this case there is a solid phase flow circuit, where appears the balance between the fuel, directed to furnace and the circulating ash. This balance is guaranteed by permanent emersion of the particles from separator and by the coarse ash from furnace.

The basic part of fluidized bed furnace is the combustion chamber with air partition grate, where the fine fuel is directed or to the grate, hovering this bed, or to the chamber at the bed, where the secondary air with big speed is given from the blast tube. The wall of the furnace chamber screened with the heat-exchange surface, so it is possible to use platen heating surface or with the form of wing heating surface. Fuel combustion, heat releasing, processes in the mineral part and the formation of the ash takes place in the bed and in the chamber on the bed, and also partly after the furnace.

The concentration of the fuel in the circulating fluidized bed is quite small (*ca* 0,5-2%), wherefore heat is released with dispersion over the whole fireplace, this is equilibrated by the heat, which is assumed evenly by the heating surface. This is the reason why there are no local high temperature areas in the furnace and therefore there is no need in installing extra heat-exchange surfaces to the beds.

The furnace of the circulating fluidized bed is adjusted by the air-fluidized bed heat exchanger, which is installed to the solid particles reflow from the separator and which work stands in very intensive heat exchange from the fluidized bed to the heating surface.

By combusting oil-shale in fluidized bed sulfur is being totally connected with ash and that is why there is almost no sulfur dioxide in the combustion gas, therefore there is no need of absorbent for tying up the sulfur or in cleaning the boiler from the sulfur. The reason consists in the fact that oil-shale has a big mole ratio Ca/S and by thermal decomposition of carbonate minerals the spare lime is generated, which is quite good sulfur binder. This is quite a good advantage for fluidized bed combusting of oil-shale.

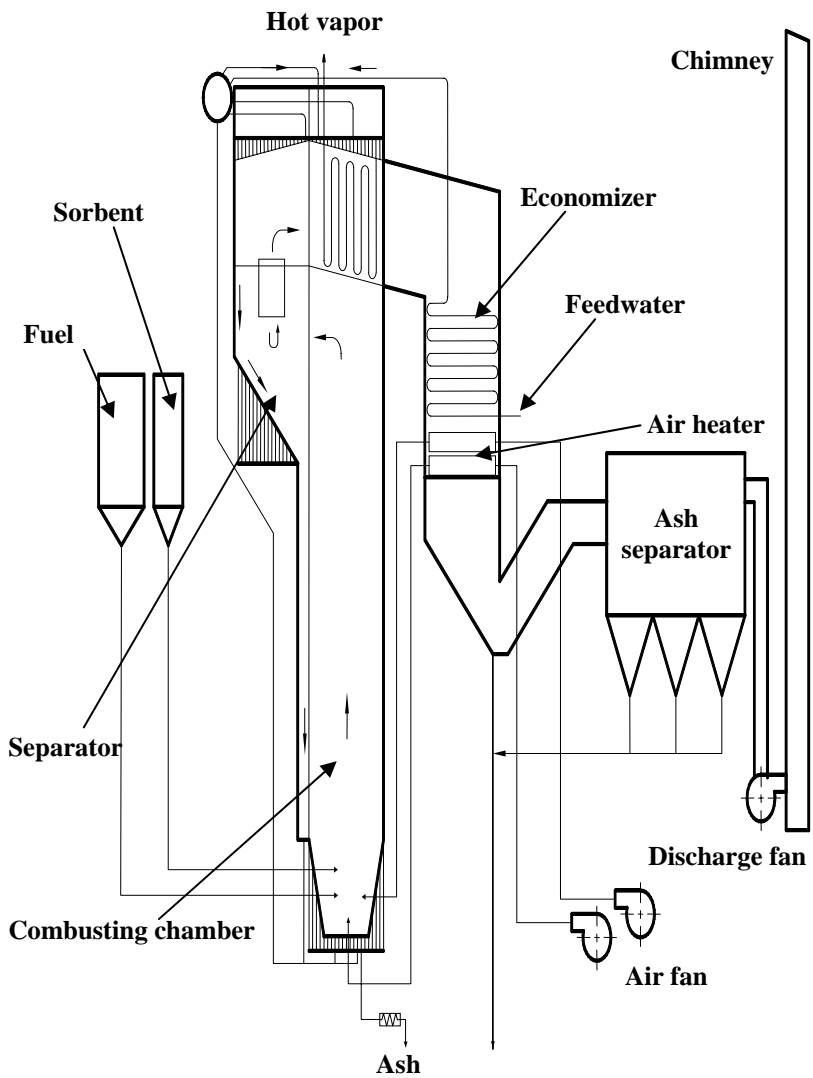


Figure 1. Circulating fluidized bed boiler with furnace internal separator [53]

On figure 1 you can see scheme of circulating fluidized bed furnace with internal separator, after which there is located boiler with convection heating surface. Separator with furnace is a one unit. Combustion gas is directed from the furnace departure window to the separator, in which caught particles head trough the furnace and separator interwall channel back to the furnace. Separator chamber panel wall is an additional heating surface.

The originality of circulating fluidized bed furnace is compression node between separator and furnace, which is used for preventing backflow of the combustion gas, as the pressure in furnace is higher than in separator. Bottom part of furnace heat screen surface may be covered with stoneware for reducing heat exchange. The walls of furnace chamber (furnace top) are water-walled.

Sectionalizing of air, which is supplied to furnace, approximates to combustion process fuel two-step burning, whereby lowering the concentration of the oxygen in upper grate chamber and with it the combustion of nitrogen oxide concentration.

The concentration of fuel in solid-phase is small, usually does not exceed 0.5-2%, so that the heat release at height in furnace is scattered and relatively steady, so there is no need in placing the heating surface to the upper grate layer. Combustion may reach the separator too.

In circulating fluidized bed furnace there is a rather complex structure of aerodynamics, which scheme is shown on figure 2.

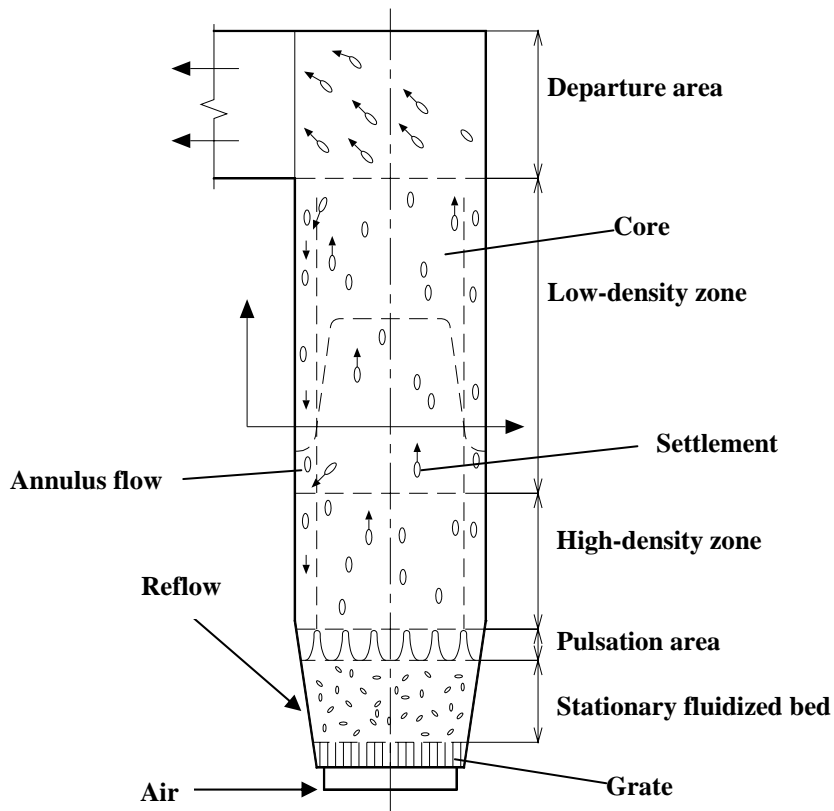


Figure 2. Internal aerodynamics in circulating fluidized bed furnace[53]

The furnace internal aerodynamics is affected by the furnace dimensions and heat input (gas velocity in furnace).

Taking into account the characteristic parameters of two-phase flow, the furnace process by height (by grate surface) could be divided into four zones. The first part is situated near the grate, high-density solid-phase, which is similar to classical fluidized bed. This zone may be in turn divided into a further layer situated directly on the grate and upper layer pulsating zone. Due to high surface velocity these parts are not so clearly separable from the rest as in case of classical fluidized bed.

The first zone is followed by the high-density upper layer zone and the solid-phase low-density area in turn. The fourth one is a departure area. Furnace internal aerodynamics in the fourth zone depends on both the furnace, as well as its geometric shape and hatch dimensions, as well as speed and density of the solid-phase hatch outside the section.

Circulating fluidized bed internal furnace two-phase flow aerodynamics affects the so-called wall effect, which appears especially in case of large appliances.

Part of outgoing particles, which departure from layer and rise up are concentrated in colonies, in which solid-phase volumetric concentration is $0.1-0.2 \text{ m}^3/\text{m}^3$. Such colonies leave the flow, bound to the wall and under gravity fall back to the layer. Particles may also have a specific cross-flow component from the wall to the centre of the furnace, but it is not of paramount importance. Particles colonies are more likely in areas where solid phase is denser and gas surface velocity is smaller (the variation of particle concentration and velocity in furnace cross-section is shown in figure 2).

The force, which influence down falling particles at layer alongside wall, is predominantly gravitational force, therefore the gas flow which rises the velocity of particles, has a small impact. In furnace arises internal circulation of particles, in which the solid phase rises up in the cross-section of the furnace and the particles colonies in layer alongside wall sink below. There is also a mass transfer in the form of solid-phase movement in radial direction, in which the diffusion of single particles is predominant in comparison with the diffusion of particle groups. Solid-phase internal furnace circulation encourages the mass and heat transfer from the furnace cross-section to the boundary layer alongside wall, intensifies the heat transition from the furnace medium to the heat-exchange surface, reduces the influence of the boundary layer alongside wall to the radiant transfer and approximates the temperature field in the furnace section.

1.1.1 Boiler heating surface fouling

Boiler heating surface fouling (blanketing of ash buildup) is a complicated effect by nature, the results of different physicochemical processes, it could not be simply explained and described, because scores of factors influence this action [53]. Most important of them – mineral and organic part formation of the fuel, transformation processes in fuel mineral part caused by combustion, fly ash breakup, ash concentration in combustion gas, combustion gas formation, temperature of combustion gas and heating surface pipes, combustion gas flow velocity, eccentricity of heating surface design, ash fouling cleaning technology etc. Tolerably substantially influences the fouling of heating surface the time factor – in the course of time the deposits structure, pressure resistance, thermo-physical properties etc. can change.

The investigation of boilers heating surface fouling figures out two purposes: to find out 1) the substance of fouling and 2) the influence of the heating surface deposit to heat transfer.

The substance of fouling of the heating surface pipes is that the solid particles carry from the gaseous environment to the heating surface, besides the condensation of the components which are in the steam phase (if there are suitable conditions). In this

process there is important the granular partition of the ash particles, velocity of the combustion gas and its formation (the partial pressure of sulfur dioxide and oxygen).

Whereas the combustion gas temperature and also velocity and other conditions are not constant along gas travel of boiler, then also fouling conditions of heating surface (within gas travel) are not the same, wherefore the properties of pipes deposits can change grossly and on the oil-shale boiler heating surface there are seen different types of ash deposit.

1.1.2 Oil-Shale ash properties

In 2007 approximately 6.5 million tons of ash was acquired as a byproduct of using oil shale for energy production. Approximately 1.5 million tons of that was ash from CFB boilers [1]. The Estonian oil shale mineral part consists mainly of the following minerals: calcite 44.0%, dolomite 19.5%, quartz 8.7%, orthoclase 10.5%, hydromuscovite 8.6%. These minerals comprise 91.3% of the mineral part and it should be noted that 63.5% of that are minerals in the carbonaceous part and 27.8% – in the terrigenous part. When oil shale is fired, thermal decomposition of these minerals occur into simpler compounds, coupled with volatilisation of some compounds and formation of novel minerals, and there are changes in the mineral phase state as well. The ash binding properties and behaviour in ash fields depend on these changes, the extent of which is determined by the firing temperature in the boiler furnace.

The short overview about behavior of fuel minerals in combustion process and formation of novel minerals and binding properties of ash is given below [1].

Carbonate minerals. The decomposition processes start at temperatures below 800°C and depend on CO₂ partial pressure in flue gas. Formed (CaO, MgO ja FeO) stay in ash free oxides and CO₂ volatilize. Decomposition of dolomite (CaMg(CO₃)₂) occurs in two steps: Mg(CO₃) decompose at lower temperatures and Ca(CO₃) at higher temperatures.

Quartz (SiO₂) does not decompose in furnace processes, but may undergo polymorphic changes in crystal structure – β-quartz changes to the α-quartz at 573°C. SiO₂ mainly appears in oil shale ash in form of α-quartz.

Orthoclase (K₂O·Al₂O₃·6SiO₂) changes to the sanidine at ~900°C, in decomposition process it forms leucite (K₂O·Al₂O₃·4SiO₂), while SiO₂ separates in form of amorphous SiO₂ or cristobalite. The presence of lime accelerates the thermal decomposition of orthoclase.

Micas are presented in oil shale as muscovite. At 120°C, absorbed water and, between 450 and 700°C, crystal water are released. In the temperature range 850 to 1,200°C (depending on the composition of micas), novel crystals are formed. Between 1,000

and 1,300°C, the liquid phase begins. At higher temperatures, corundum (Al_2O_3), mullite ($3\text{Al}_2\text{O}_3 \cdot 2\text{SiO}_2$), and glassy substance form.

Novel minerals and binding properties of ash. One of more active oil shale mineral part decomposition component is CaO, which reacts with SiO_2 and other minerals decomposition components.

The behavior and composition of Estonian oil-shale were investigated by [1]. The ash samples were taken from boilers of the Estonian Baltic Power Plant.

Table 1. Ash samples from boilers of the Estonian Power Plant [1]

Description	Bottom ash	Ash from EP field I
	CFB-boiler	CFB-boiler
Chemical analyze		
SiO_2	11.26	38.58
Fe_2O_3	3.12	4.88
Al_2O_3	4.38	11.86
CaO	48.9	27.98
CaO_v	13.88	8.36
MgO	6.37	4.53
K_2O	1.15	4.47
Na_2O	0.1	0.24
SO_3 total	13.88	4.1
CO_2	11.9	5.28
Calculated extent of carbonates decomposition		
CO_2 CaO	38.07	21.78
CO_2 MgO	6.72	4.78
CO_2 total	44.79	26.56
k_{CO_2}	0.73	0.8
Distribution of CaO between ash minerals		
CaO_{carb}	15.15	6.72
CaO_{sulf}	9.72	2.87
CaO_{free}	13.88	8.36
$\Sigma\text{CaO}_{\text{carb+sulf+free}}$	38.75	17.95
CaO_{tm}	10.15	10.03
CaO_{tm}	10.15	10.03

1.2 Fluidized beds and fluidization

Gas-particle flows in fluidized beds exhibit a number of complex characteristics (Kunii, Levenspiel 1991, [41]). Depending on the inlet conditions and particle properties, the fluidization of a bed of particles can enter into a number of different regimes. When inlet gas velocity is small, the gas will slowly seep through the particle bed. In this case, the particle bed remains fixed. At higher inlet velocities, the greater pressure drop of the fluidizing gas causes the particle bed to expand and enter a state of steady and homogeneous fluidization. Upon fluidization, the two phase suspension exhibits a fluid-like behaviour. The particular velocity at which fixed bed begins to expand is defined as the minimum fluidization velocity. Even higher gas velocities (much higher than the minimum fluidization velocity) create irregular fluidization. This may take the form of a bubbling bed, characterized by large bubbles of gas moving through a dense „emulsion” phase. In turbulent fluidization, very high inlet velocities cause further bed expansion and highly non-uniform particle concentrations within the fluidized bed. Even higher inlet velocities yet push the particles into a fast fluidization regime, where the fluidizing gas carries solids out the top of the unit. [2] Fluidized bed operations in the gas fluidization regime require additional operating units to return the entrained particles back into the system. The entire apparatus used to carry out this operation including the fluidized bed and particle recirculation system is called a circulating fluidized bed.

1.3 Overview of existing mathematical models

1.3.1 Models

The numerical simulations are mainly performed within the Lagrangian approach by the tracking of single particles or their packages in order to capture the particle-fluid interactions. For example, the two-dimensional gas-solid particles flow taken place in the CFB riser with a total volume concentration of solids 3 % has been studied in [27] by the Lagrangian approach using the particles tracking method. In the present work it is used another method - the two-fluid model, i.e. the Eulerian approach, is applied for the motion of the dispersed phase. The advantage of the Eulerian method is to obtain the distributions of all flow dynamic parameters, including the particle mass concentration. This method does not depend on the number of the tracked particles which model the motion of the disperse phase, contrary to the Lagrangian approach, which convergence is determined by the number of the tracked single particles that can be up to hundreds of thousands, and it requires high computational capabilities. An implementation of an original closure model of linear and angular momentum of polydispersed solid phase [14] based on interparticle collision in Eulerian frame allows first of all correctly described four-way coupling effect in case of highly loaded flow, secondly, to take into account particle collisions which seem to be very significant with respect of high flow mass ratio and big range of particle size deviation. Finally, implementation of our model description [35] used for calculation of pneumatic transport to conditions of fluidized bed ($T=850^{\circ}\text{C}$) considering low density

of carrier gas ($\rho = 0.27 \text{ kg/m}^3$) and its high coefficient of kinematic viscosity which is roughly 10 times larger than that at the normal conditions of $T=20^\circ\text{C}$, and the real geometry of the flow with respect of inlet size of 2.5 m allows to validate our numerical simulations and obtained results. Within the Eulerian approach the original collision model was used for closure of the transport equations by accounting the interparticle collision effect occurred in CFB due to high mass loading [27]. The numerical parametric study deals with the influence of various riser exit geometries on the hydrodynamics of the gas-solid two-phase flow taken place in the riser of CFB [66]. The problems of two-phase flows in the CFB risers are analysed in the observed publications, but these studies do not consider the dependence of amount of the sensible heat carried by the ash solid particles on their concentration in gases. In the present work the gas-solid particles flow in conditions of CFB is studied, taking into account the amount of heat, which must be separated from the combustor by the sensible heat of the ash solid ash particles. This Eulerian approach enables to optimize the concentrations of the ash solid particles in fire gases.

1.3.2 Mass conservation

The general statement for mass conservation is that the net efflux of mass from a control volume plus the rate of accumulation of mass flow in the volume is zero. The continuity equation is

$$\frac{\partial}{\partial t}(\alpha_c \rho_c) + \frac{\partial}{\partial x_i}(\partial_c \rho_c u_i) = - \sum_k^N \dot{m}_k / V = s_{mass} \quad (1.1)$$

If all droplets are evaporating at the same rate the mass source term simplifies to $s_{mass} = -\dot{m}$. Of course, the use of a differential equation implies that continuous phase properties are averaged over a volume and the averaged properties are associated with point. Obviously if the size of the averaging volume is comparable to the dimensions of the system, the differential forms of the equations are inapplicable.

1.3.3 Turbulence

Turbulence in a single-phase flow is generally characterized by the turbulence energy κ and the dissipation rate ε . This is known as the two-equation model. The equations for κ and ε are developed starting with Reynolds equations which are the equations for the fluctuating velocity components. An energy balance is formulated to calculate the level of turbulence resulting from the introduction of the particles, as shown in figure 3 [40]:

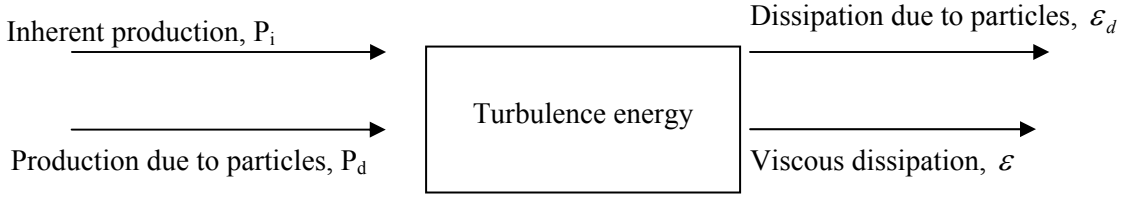


Figure 3. Schematic of model for turbulence modulation [40]

Nowadays in models for closing systems of averaged equations turbulent motion there are used equations for transferring fluctuating characteristics of content (tensor of turbulent strain, fluctuation kinetic energy, velocity of dissipation fluctuation energy).

The equation of transferring Reynolds strains [59]:

$$\begin{aligned}
 \frac{\partial}{\partial t} (\overline{V'_{gi} V'_{gk}}) + \sum_i \bar{V}_{gj} \frac{\partial}{\partial x_i} (\overline{V'_{gi} V'_{gk}}) &= \sum_i \frac{\partial}{\partial x_i} \left[\nu \frac{\partial}{\partial x_i} (\overline{V'_{gi} V'_{gk}}) - \overline{V'_{gk} V'_{gj} V'_{gi}} \right] - \\
 - \sum_i (\overline{V'_{gj} V'_{gk}} \partial V'_{gi} / \partial x_i + V'_{gj} V'_{gi} \partial V'_{gk} / \partial x_i) &- \frac{1}{\rho_g} (V'_{gk} \partial p' / \partial x_i + V'_{gi} \partial p' / \partial x_k) - \\
 - 2\nu \sum_i (\partial V'_{gk} / \partial x_i) (\partial V'_{gi} / \partial x_i) &- \rho_g^{-1} (\overline{F'_i V'_{gk}} + \overline{F'_k V'_{gi}}) \quad (1.2)
 \end{aligned}$$

On the ride side of the equation the first unit characterizes the diffusion of turbulent strains, the second – their generation (due to the lumped motion energy), third – pressure forces in fluctuation motion, fourth – dissipation of turbulent fluctuation due to the viscosity, fifth – additional dissipation of pulsation due to presence of dispersed particles.

After numerous assumptions and clever physical reasoning, an equation is developed which relates the change in turbulence energy to terms representing the diffusion of turbulence energy, generation of energy and dissipation. The generation of turbulence energy results from velocity gradients in the flow and the dissipation from viscous effects. The dissipation equation comes from taking the curl of the Reynolds equations which essentially gives the vorticity of the fluctuating velocity components. Once again the rate of change of dissipation is related to diffusion, generation and dissipation. There have been many modifications suggested to improve the $\kappa - \varepsilon$ model but the essential features remain the same and in maintains a prominent role in the commercial fluid mechanics codes (Wilcox, 1993). More recently, more attention has been developed to the turbulence models based on large eddy simulation as an improvement over the $\kappa - \varepsilon$ model.

Turbulence modulation is the effect of particles or droplets on the turbulence of the carrier phase. Modulation is weak if the particle concentration is very low. Also, at very high concentrations, near the state of a packed bed, fluid turbulence is attenuated by the large viscous forces associated with the small Reynolds number based on the interparticle spacing. These limited cases are not addressed here. While the study of the particle dispersion in turbulence has a long history, the effect of the particles on fluid turbulence has been the subject of studies conducted over the past years.

It was not until the 1970s that direct measurements of turbulence in the presence of particles were possible. Although these measurements were relatively new, practitioners in some engineering fields were already aware of the fact that the presence of particles can significantly change the rates of heat transfer and chemical reaction, which could not be explained except through the effect of the particles on the fluid turbulence. The drag reduction phenomenon observed in the pipe flows with low solids concentrations is another example which suggested that the particle phase modified the carrier phase turbulence.

The primary obstacle in obtaining fluid turbulence data in particulate flows was the difficulty with making fluid property measurements in the presence of solid particles. Before the invention of laser Doppler velocimetry (LDV), hot-wire or hot-film anemometry were the only means to acquire a direct measurement of fluid turbulence. Hot-wire probes cannot be used in flows with solid particles but a conical probe coated with a hot-film is durable, to some degree, in solid-liquid flows. For this reason the early data on fluid turbulence in the presence of solid particles were obtained in liquid-solid flows in connection with sediment transport. Some researchers attempted to use a hot-wire probe in gas-droplet free-jets in the study of a two-fluid atomizer and obtained results showing that particles (liquid droplets) suppress the turbulence intensity of gas.

Two papers (Gore&Crowe, 1989; Hetsroni 1989) summarize the available data on turbulence modulation (until 1989). These papers suggest criteria for the suppression and enhancement of turbulence. One criterion is based on the length scale ratio d/L_e , where d is the particle diameter and L_e is the length scale characteristic of the most energetic turbulent eddies. Turbulence intensity is attenuated for d/L_e less than 0,1 while the turbulence level is increased for larger length scale ratios. Another criterion is based on the relative particle Reynolds number. The model suggests that particles with a low Reynolds number tend to suppress the fluid turbulence and particles with high particle Reynolds number tend to increase turbulence.

Although some qualitative trends have been observed for the effects of particles on the turbulence energy of the carrier phase, there is currently no general model that can be used reliably to predict carrier phase turbulence in particle-laden flows.

The presence of particles can affect the carrier phase turbulence in several ways (Crowe, 1993), such as:

- displacement of the flow field by flow around a dispersed phase element,

- generation of wakes behind particles,
- dissipation of turbulence transfer of turbulence energy to the motion of the dispersed phase,
- modification of velocity gradients in the carrier flow field and corresponding change in turbulence generation,
- introduction of additional length scales which may influence the turbulence dissipation,
- disturbance of flow due to particle-particle interaction.

Numerical models for turbulence modulation are still in development so no specific model has been adopted. The general approach is to modify the generation and dissipation terms in the κ - ε equations and develop Reynolds equations for the averaged quantities. This approach leads to a fallacy (Crowe et al., 1996).

One approach which has been used to model the effect of particles on the carrier phase turbulence is direct numerical simulation (DNS). This approach is advantageous because it requires no Reynolds stress modeling. Squires and Eaton (1990) used DNS with spectral methods to study the effect of particles on isotropic, homogeneous turbulence at low Reynolds numbers. Energy had to be added to maintain the turbulence. They modeled the effect of the particles by including a point forces (drag) in the flow field. It was found that the presence of the particles increases the turbulence dissipation rate. Squires and Eaton also found that the particles tend to concentrate in regions of high strain. Elghobashi and Truesdell (1993) used a similar approach to model the effect of particles on turbulence. They also predicted that the rate of viscous dissipation is increased due to presence of the particles.

For gas-particle flows it can be shown that the energy transferred to particulate motion is negligible. The energy added per unit mass to the flow because of the dissipation of the work associated with drag is

$$\dot{E}_d = \frac{f}{\tau_V} \frac{\bar{\rho}_d}{\bar{\rho}_c} (u_1 - v_1)^2 \quad (1.3)$$

The dissipation of energy is given by

$$\varepsilon = \frac{k^{3/2}}{L_\varepsilon} \quad (1.4)$$

Where L_ε is the dissipation length scale. However, in a two-phase mixture, several new length scales are introduced, the particle size and the interparticle spacing. If the interparticle spacing is less than the intrinsic length scale for the flow, then the interparticle spacing should influence the dissipation. Kenning&Crowe defined a

„hybrid“ length scale, L_h , which approached the correct limits and used this for the dissipation length scale. They showed that the change in turbulence intensity for particles transported by air in a vertical duct should vary as,

$$\frac{\sigma - \sigma_o}{\sigma_o} = P = \left[\frac{L_h}{L_i} + \frac{L_h}{k_i^{3/2}} \frac{f}{\tau_V} \frac{\bar{\rho}_d}{\bar{\rho}_c} (u_1 - v_1)^2 \right]^{1/3} - 1 \quad (1.5)$$

where L_i and k_i are the dissipation length scale and turbulence energy in the flow without particles.

The inability to model the local details of the continuous phase is dispersed phase flow necessitates the use of averaging. The three general categories of averaging are time, volume and ensemble. The conservation equations based on volume averaging illustrate the influence of the dispersed phase on the carrier phase through the coupling terms and volume fractions of each phase. The deviations of the continuous phase velocity from the average velocity give rise to a Reynolds stress in the same manner as time averaging yields the Reynolds stress in single-phase flow. Modeling the Reynolds stress in a dispersed phase flow is complicated by the length scales associated with the dispersed phase. Also the heat transfer through the mixture involves the heat transfer through both the continuous and dispersed phases. The presence of the particles or droplets in the field affect the turbulence of the carrier phase as a result of enhanced turbulence generation and dissipation.

1.3.4 Drag viscous force

The „steady-state“ drag is the drag force which acts on the particle in a uniform pressure field when there is no acceleration of the relative velocity between the particle and the conveying fluid. The force is quantified by the drag coefficient through the equation [8] :

$$F_D = \frac{1}{2} \rho_c C_D A |u_1 - v_1| (u_1 - v_1) \quad (1.6)$$

where ρ_c is the density of the continuous (conveying) phase, C_D is the drag coefficient, A is the representative area of the droplet and u_1 and v_1 are the velocities of the continuous phase and the droplet or particle, respectively. Typically the area is projected area of the particle in the direction of the relative velocity.

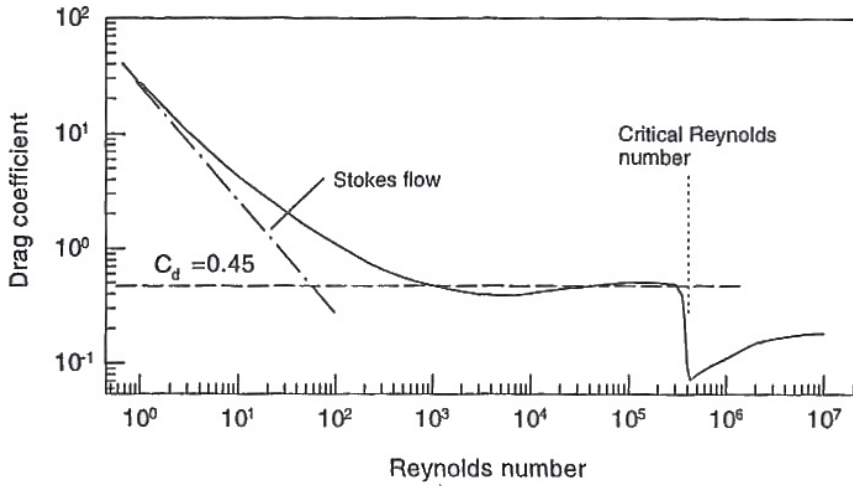


Figure 4. Variation of drag coefficient of a sphere with Reynolds number[8]

Using the drag force to solve for the drag coefficient in previous equation results in

$$C_D = \frac{24}{Re_r} \tag{1.7}$$

where Re_r is the Reynolds number based on the relative velocity. This is the classic Stokes drag coefficient which is valid for $Re_r < 1$.

An extension of Stokes analysis is the Hadamard - Rybczynski drag law for a spherical fluid particle in which the shear on the surface induces an internal motion (Clift et al., 1978, [5]). In this case the drag coefficient becomes

$$C_D = \frac{24}{Re_r} \left(\frac{1 + \frac{2}{3}\bar{\mu}}{1 + \bar{\mu}} \right) \tag{1.8}$$

where $\bar{\mu}$ is the ratio of the viscosity of the carrier phase to that of the fluid sphere. For a droplet in air, $\bar{\mu} \rightarrow 0$ and Stokes law is recovered. For a bubble in a liquid, $\bar{\mu} \rightarrow \infty$ so that the drag coefficient becomes $16/Re$.

The Stokes drag force is based on a uniform free stream velocity. The Stokes drag has to be extended to account for the effect of a nonuniform flow field by the addition of the Faxen force (Happel and Brenner, 1973, [19]),

$$F_D = 3\pi\mu_C d(u_1 - v_1) + \mu_C \pi \frac{d^3}{8} \nabla^2 u_1 \quad (1.9)$$

where ∇^2 is evaluated at the position of the particle. For a uniform flow field, the Faxen force reduces to zero. The ratio of the Faxen force to Stokes drag varies as

$$\frac{F_{Faxen}}{F_{Stokes}} \approx \left(\frac{d}{l}\right)^2 \quad (1.10)$$

where l is a characteristic length associated with the carrier flow field velocity distribution, such as the radius of curvature of the velocity distribution.

For increasing Reynolds number the inertial forces become more important and the drag coefficient is higher than Stokes drag. In 1910 Oseen extended Stokes analysis to include first-order inertial effects and concluded

$$C_D = \frac{24}{\text{Re}_r} \left(1 + \frac{3}{16} \text{Re}_r\right) \quad (1.11)$$

which is valid up to a Reynolds number of 5.

With increasing Reynolds number (≈ 100), the flow begins to separate and form vortices behind the sphere. With the formation of vortices the pressure in the wake is further reduced, increasing the form drag. Finally, as the flat portion of the C_D versus Re_r curve is approached, the drag is almost entirely due to form drag with the shear drag contributing little. In this region the drag coefficient can be approximated by a constant value of 0.45 and is referred to as Newton's drag law.

At the critical Reynolds number ($\text{Re}_r \approx 3 \times 10^5$) the boundary layer becomes turbulent and the separation point is moved rearward, sharply reducing the form drag and decreasing the drag coefficient. The phenomenon is entirely due to boundary layer effects. If the particle is rough, transition to turbulence occurs at a lower Reynolds number is less well-defined as the drop in C_D is less severe. The same trend is observed with increased free stream turbulence. If the particle has sharp edges, the separation is controlled by geometry (separation at the sharp edges) and the critical Reynolds number effect is not observed.

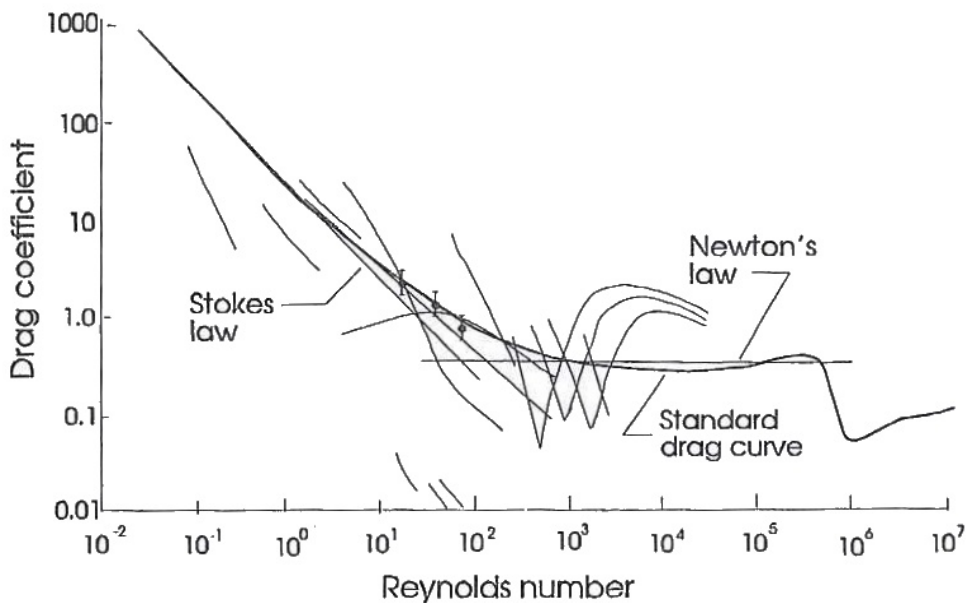


Figure 5. The spread in data obtained for the drag coefficient of a sphere [8]

1.3.5 Lift forces

Lift forces on a particle are due to particle rotation. This rotation may be caused by a velocity gradient or may be imposed from some other source such as particle contact and rebound from a surface.

1) Saffman lift force

The Saffman lift force is due to the pressure distribution developed on a particle due to rotation induced by a velocity gradient. The higher velocity on the top of the particle gives rise to a low pressure, and the high pressure on the low velocity side gives rise to a lift force.

2) Magnus force

The Magnus force is the lift developed due to rotation of the particle, which is caused by a pressure differential between both sides of the particle resulting from the velocity differential due to rotation. The rotation may be caused by sources other than the velocity gradient.

1.3.6 Buoyant force

When a body is completely submerged in a fluid, or floating so that it is only partially submerged, the resultant fluid force acting on the body is called the buoyant force [79].

A net upward vertical force results because pressure increases with depth and the pressure force acting from below are larger than the pressure forces acting from above.

Here is the desired expression for the buoyant force [49]:

$$F_B = \gamma \nabla \quad (1.12)$$

where γ is the specific weight of the fluid and ∇ is the volume of the body. The direction of the buoyant force, which is the force of the fluid on the body. Therefore, the buoyant force has a magnitude equal to the weight of the fluid displaced by the body and is directed vertically upward.

1.3.7 Particle-particle and particle-wall interactions

Particle-particle interaction controls the motion of particles in dense particle flows. Also particle-wall interaction is important in dense flows as well as wall-dominated dilute flows.

Particle-wall interaction

The problem of particle-wall interaction is encountered when analyzing gas-particle flows contained within walls such as pipe flows, channel flows and fluidized beds. The particle-wall interaction considered here falls into two categories: hydrodynamic forces due to the proximity of a wall and the purely mechanical interaction in the absence of a fluid. The Saffmann lift force due to velocity gradient near the wall is one example of the hydrodynamic interaction. Another example is the fluid force acting on a particle approaching the wall in the normal direction.

The treatment of the mechanical behaviour associated with particle-wall interaction depends on the inertia of the particle. When a massive particle collides with a wall, it rebounds but loses kinetic energy due to friction and inelasticity effects. For a very small particle approaching a wall, molecular forces become dominant compared with the inertial force. As a result, the particle is captured by the wall due to cohesive forces, and neither rebounds from nor slides along the wall. This cohesive force is identified as the van der Waals force.

Particle-particle interaction

Particle-particle collision is negligible in dilute gas-particle flows. As the particle concentration becomes higher, particles collide with each other and the loss of particle kinetic energy due to inter-particle collision cannot be neglected. Fortunately, as long as the particulate phase is dispersed, it is sufficient to consider only simple binary collisions, not multiple collisions.

Particle-particle interaction is the key element in dense phase flows. The two models for particle-particle interaction are the hard sphere and soft sphere models. With the hard sphere model the post-collisional velocities and rotations are determined as a function of the pre-collisional conditions, coefficient of restitution and coefficient of friction. The soft sphere model describes the particle history during the collision process and can be modeled with spring-damper arrangements. Particle-wall collisions are treated with the hard sphere model. A number of theoretical investigations devoted to study of interparticle collision effect can be formally divided by the use of either Lagrangian or Euler approaches. Sommerfeld [63] presented a number of diagrams for the average and r.m.s. velocity shapes, which were obtained for a relatively large mean flow velocity, with no noticeable effect on the velocity profiles due to the particle accumulation on the bottom wall. Sommerfeld and Zivkovic [74] estimated the effect of the particles' collision on a stochastic approach using a Lagrange frame of reference. The stochastic approach for the particles' collisionmodel was also considered by Oesterle and Petitjean [51] as well as by Yamomoto et al. [77]. The calculations in the last three studies were restricted to short pipe lengths. In similar studies, Simonin and coworkers [60,61] have used the pdf approach, within the frame of the two-fluid model, to model gas-solid flows with collisions. The effect of inter-particle collisions is obviously important for dense particulate flows where the ratio of particle response time is larger than the time of inter-particle collisions that is when $\tau / t_c > 1$ with

$\tau = \left(\frac{18\rho\nu}{\rho_p d^2} C_D \right)^{-1}$ being the particle response time. The frequency of particulate collision $f_c = 1/t_c$ may be calculated by the classical expression of Marble (1967):

$$f_c = \left(\frac{d_i + d_j}{2} \right)^2 |\vec{V}_i - \vec{V}_j| n_{ij} \quad (1.13)$$

where d_i and d_j are the diameters of colliding particles, V_i and V_j are the velocities of the particles and n_{ij} is the concentration (number of particles per unit volume) of the group of particles “j,” which may collide with the group of particles “i.” An order of magnitude estimate shows that the inequality $\tau / t_c > 1$ is satisfied when the mass loading is higher than 10. Hence, interparticle collisions play an important role in the transport processes when the loading ratio is higher than 10. There are a few particle collision models obtained in a Eulerian frame of reference, such as the ones by Louge et al. [43], and Cao and Ahmadi [3]. In this paper, we also apply a two-fluid approach using a two-way coupling model. We introduce a collision model that considers the exchange of not only the linear momentum, but also the angular momentum. Hence, we obtain analytical formulae for the stress tensor components and the pseudoviscosity coefficients, using an average procedure over the collision coordinates [36]. Wall roughness can be simulated with a local wall slope at the surface.

1.4 Purposed solution

Tallinn University of Technology has a big experience in investigating two-phase flows. Lately two PhD works were done: „Effect of Solid Particles on Turbulence of Gas in Two-Phase Flows“ (Medhat Hussainov, 2005) and „Deposition of Solid Particles from Aerosol Flow in Laminar Flat-Plate Boundary Layer“ (Sergei Tisler, 2006). These works were investigating the theoretical part of the two-phase flows problem. Current work is investigating the practical point, taking in advance the data of the real Oil-Shale CFB power plant in Narva.

2 TURBULENT BOUNDARY LAYER AND TWO-DIMENSIONAL REYNOLDS AVERAGED NAVIER-STOKES MODELING

2.1 Main predictions

2.1.1 Turbulent Boundary Layer

The numerical simulation has been performed within the two-phase turbulent boundary layer (TBL) approach. This implies that the diffusive source terms were only retained in one direction, namely in transverse direction, and magnitude of the average transverse velocity components of the gas- and dispersed phases were much less than that of the longitudinal components of the corresponding velocities of both phases. Such approach is thoroughly valid and used in the pipe channel flows as well as in the turbulent round jets together with the flow past of the rigid shapes [28], [29].

To make calculations we applied the two-fluid model assuming the dispersed phase to be the continuous phase like a carrier fluid (in our case it was the gas phase) but having its own flow parameters such as the velocities, concentration etc., which differ from that of the carrier fluid. Actually, the dispersed phase is the polydispersed therefore we modelled its motion by the motion of the finite number of the particle fractions. In order to simplify the numerical simulations we brought into consideration three particle fractions characterized by their own mass fractions and particle sizes in order to take into account the interparticle collisions along with other force factors [35]. The collision effect is characterized here by introducing the so-called pseudo-viscosity coefficients, ν_{ci} , D_{ci} , where the diffusion coefficient of particles D_{ci} is due to their collisions and similar to the coefficient of the turbulent diffusion of particles appeared in the differential equation of the particle mass conservation (Eq. (2.2)). Among the other force factors included in the model are the drag force determined by the particle response time, τ_i , the lift Magnus and Saffman forces characterized by the rotation parameter, Ω_i , the gravitation force designated by the gravitation acceleration, g . In our modeling we applied the four-way coupling model of [7] which allows to take into account both generation and attenuation of turbulence of gas by particles.

2.1.2 2-Dimensional Reynolds Averaged Navier-Stokes

“Two-fluid model” is being used in the modeling of dispersed two-phase systems, where the gas and the particles are considered as two coexisting phases that reach the entire flow domain. To describe the flow of the particulate phase, one of the possibilities is using the Reynolds Averaged Navier-Stokes (RANS) method. The general equations of this method were examined by plenty of experiments, which showed, that using this method it is possible to discover, for example, boundary conditions and it is quite easy to implement it numerically. In this work we use the RANS method with it’s closure equations to find on the output needful data: axial and radial velocities, turbulent energy, mass concentration. The information on these parameters will surely be useful for particulate slow predictions.

2.2 Governing equations

2.2.1 Turbulent Boundary Layer equations

The governing TBL equations presented in the tensor form are the following (here “i” is the order number of the particles fractions, i=1,3):

Continuity equation for the gas phase:

$$\frac{\partial u}{\partial x} + \frac{\partial(rv)}{r\partial r} = 0 \quad (2.1)$$

Linear momentum equation in the axial direction for the gaseous phase:

$$u \frac{\partial u}{\partial x} + v \frac{\partial u}{\partial r} = \frac{\partial}{\partial r} r(v_t + v) \frac{\partial u}{\partial r} - \frac{dp}{\rho dx} - \sum_{i=1,3} \alpha_i \left[C'_{Di} \frac{(u - u_{si})}{\tau_i} + C_{Mi} \left(\omega_{si} - \frac{\partial u}{2\partial r} \right) (v - v_{si}) \right] \quad (2.2)$$

Equation for the radial velocity of gas phase obtained as result of a combine solution of equations (2.1) and (2.2) is:

$$v = -\frac{u}{r} \int_0^r \frac{r}{u^2} \left\{ \frac{\partial}{\partial r} r(v_t + v) \frac{\partial u}{\partial r} - \frac{dp}{\rho dx} - \sum_{i=1,3} \alpha_i \left[C'_{Di} \frac{(u - u_{si})}{\tau_i} + C_{Mi} \left(\omega_{si} - \frac{\partial u}{2\partial r} \right) (v - v_{si}) \right] \right\} dr \quad (2.3)$$

The pressure drop is obtained from eq. (3) and is the following:

$$\frac{dp}{\rho dx} = \frac{\int_0^R \frac{r}{u^2} \left\{ \frac{\partial}{\partial r} r(v_t + v) \frac{\partial u}{\partial r} - \sum_{i=1,3} \alpha_i \left[C'_{Di} \frac{(u - u_{si})}{\tau_i} + C_{Mi} \left(\omega_{si} - \frac{\partial u}{2\partial r} \right) (v - v_{si}) \right] \right\} dr}{\int_0^R \frac{r dr}{u^2}} \quad (2.4)$$

Turbulence kinetic energy equation for the gaseous phase:

$$u \frac{\partial k}{\partial x} + v \frac{\partial k}{\partial r} = \frac{\partial}{\partial r} r \left(\frac{v_t}{\sigma_t} + v \right) \frac{\partial k}{\partial r} + \sum_{i=1,3} \alpha_i \left[\frac{(u - u_{si})^2}{\tau_i} + k_{sci} - (\overline{u'u'_{si}} + \overline{v'v'_{si}} + \overline{u'v'_{si}} + \overline{v'u'_{si}}) \right] - \varepsilon_h \quad (2.5)$$

Mass conservation equation of the solid phase:

$$\frac{\partial(\alpha_i u_{si})}{\partial x} + \frac{\partial}{r \partial r} r \left[\alpha_i v_{si} - (D_{si} + D_{ci}) \frac{\partial \alpha_i}{\partial r} \right] = 0 \quad (2.6)$$

Momentum equation in the axial direction for the solids phase:

$$\begin{aligned} \alpha_i u_{si} \frac{\partial u_{si}}{\partial x} + \left[\alpha_i v_{si} - (D_{si} + D_{ci}) \frac{\partial \alpha_i}{\partial r} \right] \frac{\partial u_{si}}{\partial r} = \frac{\partial}{r \partial r} r \left(\alpha_i v_{si} \frac{\partial u_{si}}{\partial r} \right) - \\ - \sum_{i=1,3} \alpha_i \left[C'_{Di} \frac{(u - u_{si})}{\tau_i} + C_{Mi} \left(\omega_{si} - \frac{\partial u}{2 \partial r} \right) (v - v_{si}) \right] - \left(1 - \frac{\rho}{2 \rho_p} \right) g \end{aligned} \quad (2.7)$$

Momentum equation in the radial direction for the solids phase:

$$\begin{aligned} \alpha_i u_{si} \frac{\partial v_{si}}{\partial x} + \left[\alpha_i v_{si} - (D_{si} + D_{ci}) \frac{\partial \alpha_i}{\partial r} \right] \frac{\partial v_{si}}{\partial r} = \frac{\partial}{r \partial r} r \left(\alpha_i v_{si} \frac{\partial v_{si}}{\partial r} \right) - \\ - \sum_{i=1,3} \alpha_i \left\{ C'_{Di} \frac{(v - v_{si})}{\tau_i} - \left[C_{Mi} \left(\omega_{si} - \frac{\partial u}{2 \partial r} \right) + F_s \right] (u - u_{si}) \right\} \end{aligned} \quad (2.8)$$

Linear moment-of-momentum equation for the dispersed phase:

$$\begin{aligned} u_{si} \frac{\partial(\alpha_i \omega_{si})}{\partial x} + \left[\alpha_i v_{si} - (D_{si} + D_{ci}) \frac{\partial \alpha_i}{\partial r} \right] \frac{\partial(\alpha_i \omega_{si})}{\partial r} = \\ = \frac{\partial}{r \partial r} \left(r \alpha_{si} v_{si}^{\omega} \frac{\partial \omega_{si}}{\partial r} \right) - \frac{\alpha_i C_{\omega i}}{\tau_i} \left(\omega_{si} - \frac{\partial u}{2 \partial r} \right) \end{aligned} \quad (2.9)$$

Here Eq. (2.1) is the continuity equation, Eq. (2.4) is the mass conservation equation of the polydispersed phase, Eqs. (2.2) and (2.5) presented in the tensor form cover the momentum exchange for the longitudinal and radial directions for the gas and polydispersed phases, respectively. The closure of the momentum equations is performed by the transport equation of the turbulent energy (Eq. (2.3)) derived by Crowe & Gilland (1998).

2.2.2 2-Dimensional Reynolds Averaged Navier-Stokes equations

This model is based on the complete averaged Navier-Stokes equations (the equations of motion for fluid flow), without any simplifications, such as “boundary layer” simplifications. A short presentation of the governing equations for the axis-symmetric pipe case is as follows:

1. Continuity equation for the gas phase:

$$\frac{\partial u}{\partial x} + \frac{\partial(rv)}{r\partial r} = 0 \quad (2.10)$$

2. Linear momentum equation in the axial direction for the gaseous phase:

$$\begin{aligned} & \frac{\partial}{\partial x} \left[u^2 - (v_t + v) \frac{\partial u}{\partial x} \right] + \frac{\partial}{r\partial r} r \left[uv - (v_t + v) \frac{\partial u}{\partial r} \right] = \\ & = -\frac{\partial p}{\rho\partial x} + \frac{\partial}{\partial x} (v_t + v) \frac{\partial u}{\partial x} + \frac{\partial}{r\partial r} r (v_t + v) \frac{\partial v}{\partial x} - \\ & - \sum_{i=1,3} \alpha_i \left(\frac{u_{ri}}{\tau'_i} + C_{Mi} \Omega_i v_{ri} \right) \end{aligned} \quad (2.11)$$

3. Linear momentum equation in the radial direction for the gaseous phase:

$$\begin{aligned} & \frac{\partial}{\partial x} \left[uv - (v_t + v) \frac{\partial v}{\partial x} \right] + \frac{\partial}{r\partial r} r \left[v^2 - (v_t + v) \frac{\partial v}{\partial r} \right] = \\ & = -\frac{\partial p}{\rho\partial r} + \frac{\partial}{\partial x} (v_t + v) \frac{\partial u}{\partial r} + \frac{\partial}{r\partial r} r (v_t + v) \frac{\partial v}{\partial r} - \\ & - \frac{2v_t v}{r^2} - \sum_{i=1,3} \alpha_i \left(\frac{v_{ri}}{\tau'_i} - (C_{Mi} \Omega_i + F_{si}) u_{ri} \right) \end{aligned} \quad (2.12)$$

4. Turbulence kinetic energy equation for the gaseous phase:

$$\begin{aligned} & \frac{\partial}{\partial x} \left[uk - (v_t + v) \frac{\partial k}{\partial x} \right] + \frac{\partial}{\partial r} \left[vk - (v_t + v) \frac{\partial k}{\partial r} \right] = \\ & = v_t \left\{ 2 \left[\left(\frac{\partial u}{\partial x} \right)^2 + \left(\frac{\partial(rv)}{r\partial r} \right)^2 \right] + \left(\frac{\partial u}{\partial r} + \frac{\partial v}{\partial x} \right)^2 \right\} - \\ & - \varepsilon_h + \sum_{i=1,3} \frac{\alpha_i}{\tau_i} \left(u_{ri}^2 + v_{ri}^2 + 0.5(\overline{u_{si}^2} + \overline{v_{si}^2})_c - \frac{k}{\left(1 + \frac{\tau_i}{T_0} \right)} \right) \end{aligned} \quad (2.13)$$

6. The coefficient of the turbulent viscosity:

$$\nu_t = \frac{k^2}{\varepsilon_0} \quad (2.14)$$

7. The rate of dissipation of the turbulent energy of the gaseous phase by four-coupling model:

$$\varepsilon_h = \frac{2\lambda L_0}{\lambda + L_0}, \quad (2.15)$$

where the inter-particle spacing is

$$\lambda = \delta_i \left(\sqrt[3]{\frac{\pi\rho_p}{6\rho\alpha_i}} - 1 \right) \quad (2.16)$$

integral turbulence length scale calculated for single phase pipe is

$$L_0 = \frac{k_0^{3/2}}{\varepsilon_0} \quad (2.17)$$

k_0 and ε_0 are the turbulent energy and its rate of dissipation of single phase pipe flow.

8. *Momentum equation in the axial direction for the dispersed phase:*

$$\begin{aligned} \frac{\partial}{\partial x} \alpha_i \left(u_{si} \tilde{u}_{si} - v_{si}^{xx} \frac{\partial u_{si}}{\partial x} \right) + \frac{\partial}{r \partial r} r \alpha_i \left(u_{si} \tilde{v}_{si} - v_{si}^{xr} \frac{\partial u_{si}}{\partial x} \right) &= \frac{\partial}{\partial x} \left(\alpha_i v_{si}^{xx} \frac{\partial u_{si}}{\partial x} \right) + \\ + \frac{\partial}{r \partial r} \left(r \alpha_i v_{si}^{xr} \frac{\partial v_{si}}{\partial x} \right) + \alpha_i \left[\frac{u_{ri}}{\tau'_i} + C_{Mi} \Omega_i v_{ri} - g \left(1 - \frac{\rho}{2\rho_p} \right) \right] & \quad (2.18) \end{aligned}$$

9. *Momentum equation in the radial direction for the dispersed phase:*

$$\begin{aligned} \frac{\partial}{\partial x} \alpha_i \left(v_{si} \tilde{u}_{si} - v_{si}^{xr} \frac{\partial v_{si}}{\partial x} \right) + \frac{\partial}{r \partial r} r \alpha_i \left(v_{si} \tilde{v}_{si} - v_{si}^{rr} \frac{\partial v_{si}}{\partial x} \right) &= \frac{\partial}{\partial x} \left(\alpha_i v_{si}^{xr} \frac{\partial u_{si}}{\partial r} \right) + \\ + \frac{\partial}{r \partial r} \left(r \alpha_i v_{si}^{rr} \frac{\partial v_{si}}{\partial x} \right) - \frac{2\alpha_i v_{si}^{rr} v_{si}}{r^2} + \alpha_i \left[\frac{v_{ri}}{\tau'_i} + (C_{Mi} \Omega_i + F_{si}) u_{ri} \right] & \quad (2.19) \end{aligned}$$

10. Linear moment-of-momentum equation for the dispersed phase:

$$\frac{\partial}{\partial x} \alpha_i \left(\omega_{si} \tilde{u}_{si} - v_{si}^{\omega x} \frac{\partial \omega_{si}}{\partial x} \right) + \frac{\partial}{r \partial r} r \alpha_i \left(\omega_{si} \tilde{v}_{si} - v_{si}^{\omega r} \frac{\partial \omega_{si}}{\partial x} \right) = -\alpha_i C_{oi} \frac{\Omega_i}{\tau_i} \quad (2.20)$$

where drift velocity components of dispersed phase in the axial and in the radial directions are as the follow:

$$\tilde{u}_{si} = u_{si} - (D_{si} + D_{ci}^x) \frac{\partial \ln \alpha_i}{\partial x}, \quad \tilde{v}_{si} = v_{si} - (D_{si} + D_{ci}^r) \frac{\partial \ln \alpha_i}{\partial r} \quad (2.21)$$

3 MODEL APPLICATIONS

3.1 Numerical simulation

In a frame of turbulent boundary layer (TBL) all equations are written in numerical sample using up-wind finite difference scheme. The up-wind difference scheme has physical basis and is first order numerical scheme. The solver for the TBL equations is a tridiagonal matrix algorithm (TDMA) or Thomas algorithm with using different type of boundary conditions – at the axis (asymmetry boundary conditions) – it is set Neumann or zero gradient boundary conditions, at the wall it is a mixture of Dirichlet boundary conditions for the gas phase linear velocities and Robin boundary conditions for dispersed phase velocities and particle mass concentration. The numerical sample is

$$\begin{aligned}
 & u_j^i \left(\frac{(u_j^i - u_j^{i-1})}{\Delta x} + \frac{|v_j^i|}{\Delta r} + \frac{2k_1 + k_2 + k_3}{2(\Delta r)^2} \right) + u_{j+1}^i \left(\frac{v_j^i - |v_j^i|}{2\Delta r} - \frac{k_1 + k_2}{2(\Delta r)^2} \right) + \\
 & + u_{j-1}^i \left(\frac{v_j^i + |v_j^i|}{2\Delta r} - \frac{k_1 + k_3}{2(\Delta r)^2} \right) = f_j^i
 \end{aligned} \tag{3.1}$$

here Δx and Δr are numerical mesh sizes, respectively; u_j^i and v_j^i are unknown flow parameters, the axial and radial velocities at grid points (i, j). An upper index “i” corresponds to the axial coordinate change and lower index “j” corresponds to the radial coordinate change.

The TDMA (tridiagonal matrix algorithm) are written in general form as follows:

$$-A_m W_{m+1} + B_m W_m - C_m W_{m-1} = D_m \tag{3.2}$$

where the following conditions imposed on the coefficients of algebraic equation are as follows: $A_m > 0$, $B_m > 0$, $C_m > 0$ and $B_m > A_m + C_m$. Then one can receive solution for variable, W which is:

$W_m = E_m W_{m+1} + F_m$, where we have expressions

$$E_m = \frac{A_m}{B_m - C_m E_{m-1}} \tag{3.3}$$

$$F_m = \frac{D_m + C_m E_{m-1}}{B_m - C_m E_{m-1}} \tag{3.4}$$

In considered case where $W_m \equiv u_j^i$ the coefficients are

$$A_m = \frac{|v_j^i| - v_j^i}{2\Delta r} + \frac{k_1 + k_2}{2(\Delta r)^2} \quad (3.5)$$

$$C_m = \frac{k_1 + k_3}{2(\Delta r)^2} - \frac{(v_j^i + |v_j^i|)}{2\Delta r} \quad (3.6)$$

$$B_m = \frac{u_j^i}{\Delta x} + \frac{|v_j^i|}{\Delta r} + \frac{2k_1 + k_2 + k_3}{2(\Delta r)^2} \quad (3.7)$$

$$D_m = u_j^i \frac{u_{j-1}^i}{\Delta x} + f_j^i \quad (3.8)$$

The boundary conditions on the one side border, let's say on the left side pipe wall are following:

i) For Dirichlet boundary conditions it is set $W_1 = E_1 W_2 + F_1$ or for $W_1 = a_1$, we determine corresponding coefficients as follows: $E_1 = 0$, $F_1 = a_1$.

ii) For Neumann boundary conditions we have: $\frac{\partial \psi}{\partial y} = s_1$ or $\psi_2 - \psi_1 = s_1 \Delta y$, or

$W_1 = W_2 - s_1 \Delta y$ and comparing this equation with equation $W_1 = E_1 W_2 + F_1$ the we find unknown coefficients: $E_1 = 1$, $F_1 = -s_1 \Delta y$.

ii) For Neumann boundary conditions we have: $\frac{\partial \psi}{\partial y} = s_1$ or $\psi_2 - \psi_1 = s_1 \Delta y$, or $W_1 = W_2 - s_1 \Delta y$ and comparing this equation with equation $W_1 = E_1 W_2 + F_1$ then we find unknown coefficients: $E_1 = 1$, $F_1 = -s_1 \Delta y$.

iii) In case if we have Robin bounday condition, namely, $\psi + p_1 \frac{\partial \psi}{\partial y} = q_1$ or

$\psi_1 + p_1 \frac{\psi_2 - \psi_1}{\Delta y} = q_1$ or $W_1 = -\frac{p_1 / \Delta y}{1 - (p_1 / \Delta y)} W_2 + \frac{q_1}{1 - (p_1 / \Delta y)}$, since $\psi \equiv W$. Then

comparing last equation with equation of $W_1 = E_1 W_2 + F_1$ we find coefficients:

$E_1 = -\frac{p_1 / \Delta y}{1 - (p_1 / \Delta y)}$ and $F_1 = -\frac{q_1}{1 - (p_1 / \Delta y)}$. Obviuolsly that $\frac{p_1}{\Delta y} \neq 1$.

Then comparing it with equation, $W_1 = E_1 W_2 + F_1$ we have expressions for coefficients:

The boundary conditions on the other side border, let's say on the right side of the pipe wall can be written as follows:

i) For Dirichlet boundary conditions it is set $W_{M-1} = E_{M-1}W_M + F_{M-1}$ or for $\psi_M = a_M$, we determine the value: $W_M = a_M$

ii) For Neumann boundary conditions we have: $\frac{\partial \psi}{\partial y} = s_M$ or $\psi_{M-1} = \psi_M - s_M \Delta y$, then

comparing this equation with equation $W_{M-1} = E_{M-1}W_M + F_{M-1}$ then we find

$$W_M = \frac{F_{M-1} + s_M \Delta y}{1 - E_{M-1}}.$$

iii) In case of combined boundary conditions we have Robin's boundary conditions:

$$\psi + p_M \frac{\partial \psi}{\partial y} = q_M \text{ or}$$

$$W_M = \frac{F_{M-1} + q_M (p_M / \Delta y)}{[1 + (p_M / \Delta y)](p_M / \Delta y) - E_{M-1}} = \frac{F_{M-1} + (q_M \Delta y / p_M)}{1 + (\Delta y / p_M) - E_{M-1}} \quad (3.9)$$

Thus, we have two runs using the left side boundary conditions we determine the coefficients E and F along pipe width and then applying to the right side boundary conditions we determine the flow parameters running reverse procedure through the pipe cross-section.

The other method is applied for solution of 2D RANS system equations which renders the finite volume method. This finite (or control) volume uses the ILU (implicit lower and upper matrix) scheme with presentation of differential equations in the following form:

$$\begin{aligned} & \frac{\partial(\rho^* \Phi)}{\partial t} dV + \left[C_{x,e}^* \Phi_e - \Gamma_{\Phi,e}^* \left(\frac{\partial \Phi}{\partial x} \right)_e dy \right] - \left[C_{x,w}^* \Phi_w - \Gamma_{\Phi,w}^* \left(\frac{\partial \Phi}{\partial x} \right)_w dy \right] + \\ & \left[C_{y,n}^* \Phi_n - \Gamma_{\Phi,n}^* \left(\frac{\partial \Phi}{\partial x} \right)_n dx \right] - \left[C_{y,s}^* \Phi_s - \Gamma_{\Phi,s}^* \left(\frac{\partial \Phi}{\partial x} \right)_s dx \right] = S_\Phi dV \end{aligned} \quad (3.10)$$

in considered case there is a stationary flow with no derivation along the time, i.e.

$$\frac{\partial}{\partial t} \equiv 0.$$

Here starred variables indicate values from the previous iteration. The lower subscript indicates east (e) and west (w) and north (n) and south (s) grid directions and variable Φ is flow parameter: velocity or concentration or turbulent energy and its rate of dissipation. The mass fluxes in the x- and y- directions are defined as, $C_x = \rho u dy$ and $C_y = \rho v dx$ and they are interpolated and stored at the control volume faces: $\Phi_e = (1 - f_{x,P})\Phi_P + f_{x,P}\Phi_E$. The interpolation factor is defined as:

$$f_{x,P} = f_{x,i} = \frac{x_e - x_P}{x_E - x_P} = \frac{x_i - x_{i-1}}{x_{i+1} - x_{i-1}} \quad (3.11)$$

The diffusivities Γ_Φ and source term S_Φ are evaluated from the previous iteration. The capital index relates to center of control volume and the small index relates to the face surface of control volume. The above written differential equation is solved by two steps:

i) the fluxes through the control volume boundaries are expressed as the product of a mean flux per unit area associated with cell-face center and the cell-face area; ii) the integrated source terms and time derivatives within the control volume are expressed as the product of a mean value, associated with the cell centre, and the cell volume.

Following up-wind differencing scheme one can determine variables at the control volume surfaces:

$$\Phi_e = \begin{cases} \Phi_P & C_{x,e}^* > 0 \\ \Phi_E & C_{x,e}^* < 0 \end{cases} \quad (3.12)$$

or can be presented as

$$C_{x,e}^* \Phi_e = \max[C_{x,e}^*, 0] \Phi_P - \max[-C_{x,e}^*, 0] \Phi_E \quad (3.13)$$

Following this procedure we can write rest of variable at the control volume surfaces:

$$C_{y,n}^* \Phi_n = \max[C_{y,n}^*, 0] \Phi_P - \max[-C_{y,n}^*, 0] \Phi_N, \text{ etc.} \quad (3.14)$$

The discretization of the diffusive terms gives:

$$\left(\frac{\partial \varphi}{\partial x} \right)_e = \frac{\varphi_E - \varphi_P}{\Delta x_e}, \quad \left(\frac{\partial \varphi}{\partial y} \right)_n = \frac{\varphi_N - \varphi_P}{\Delta y_n} \quad (3.15)$$

The discretization of the source term gives

$S_\phi dV \approx S_{\phi,P} dV$, where control volume is $dV = dx \cdot dy$ (for considered 2D case). Then final discretization is

$$a_P \Phi_P = a_W \Phi_W + a_E \Phi_E + a_S \Phi_S + a_N \Phi_N + b_P \quad (3.16)$$

or in (i,j) notations it reads:

$$a_P^{i,j} \Phi_{i,j} = a_W^{i,j} \Phi_{i-1,j} + a_E^{i,j} \Phi_{i+1,j} + a_S^{i,j} \Phi_{i,j-1} + a_N^{i,j} \Phi_{i,j+1} + b_P^{i,j} \quad (3.17)$$

where finite volume coefficients are:

$$a_W^{i,j} = \max \left[C_{x,w}^*, 0 \right] + \frac{\Gamma_{\phi,w}^* dy}{\Delta x_w} \quad (3.18)$$

$$a_E^{i,j} = \max \left[-C_{x,e}^*, 0 \right] + \frac{\Gamma_{\phi,e}^* dy}{\Delta x_e} \quad (3.19)$$

$$a_S^{i,j} = \max \left[C_{y,s}^*, 0 \right] + \frac{\Gamma_{\phi,s}^* dx}{\Delta y_s} \quad (3.20)$$

$$a_N^{i,j} = \max \left[-C_{y,n}^*, 0 \right] + \frac{\Gamma_{\phi,n}^* dx}{\Delta y_n} \quad (3.21)$$

and

$$a_P^{i,j} = a_W^{i,j} + a_E^{i,j} + a_S^{i,j} + a_N^{i,j} - S_P^{i,j} dV \quad (3.22)$$

Incomplete lower „L” and upper „U” matrix decomposition method (ILU method) or Stone’s method is used for determination of unknown flow parameters (linear and angular velocities, pressure, concentration). Another words, an idea of approximate LU factorization of matrix A as iteration of matrix M is used: $M=LU=A+N$, and N is small matrix. Final expressions for element of lower and upper matrices are as follows:

$$L_W^l = \frac{A_W^l}{1 + \alpha U_N^{l-N_j}} \quad (3.23)$$

$$L_S^l = \frac{A_S^l}{1 + \alpha U_E^{l-1}} \quad (3.24)$$

$$L_P^l = A_P^l + \alpha \left(L_W^l U_N^{l-N_j} + L_S^l U_E^{l-1} \right) - L_W^l U_E^{l-N_j} - L_S^l U_N^{l-1} \quad (3.25)$$

$$U_N^l = \frac{A_N^l - \alpha L_W^l U_N^{l-N_j}}{L_P^l} \quad (3.26)$$

$$U_E^l = \frac{A_E^l - \alpha L_S^l U_E^{l-1}}{L_P^l} \quad (3.27)$$

Any matrix element that carries the index of a boundary node must be zero. Thus, along the west boundary ($i=2$), elements with index $(l-N_j)$ are zero; along the south boundary ($j=2$), elements with index $l-1$ are zero; along the north boundary ($j=N_j-1$), elements with index $l+1$ are zero; finally, along the east boundary ($i=N_i-1$), elements with index $l+N_j$ are zero. Now following to (Ferziger and Peric, 1996) the equation for residual $\delta = [\varphi]^v - [\varphi]^{v-1}$ update is,

$$LU\delta^{n+1} = \rho^n \quad (3.28)$$

Multiplication of this equation by L^{-1} leads to

$$U\delta^{n+1} = L^{-1}\rho^n = R^n \quad (3.29)$$

where R^n is easily computed

$$R^l = \frac{\rho^l - L_S^l \rho^{l-1} - L_W^l \rho^{l-N_j}}{L_P^l} \quad (3.30)$$

This equation is solved by marching in the order of increasing l . When the computation of R is complete, it is need to solve equation for residual:

$$\delta^l = R^l - U_N^l R^{l+1} - U_E^l R^{l+N_j} \quad (3.31)$$

in order of decreasing index l . In this method the elements of the matrices L and U need be calculated only once, prior to the first iteration. On the subsequent iterations one need to calculate only residual, then R and finally δ , by solving the two tridiagonal systems. This method (or Stone's method) converges in a small number of iterations. The rate of convergence determines mainly by parameter α which is used in considered modeling as $\alpha = 0.92$.

These two assumptions show the difference between control volume method and finite difference scheme where for the finite difference differential equations are approximated at each grid point replacing the particle derivatives by the nodal values

of the functions. The result is algebraic equations per grid node in which the variable value at that and a certain number of neighbor nodes appear as unknowns. Taylor series expansion or polynomial fitting is used to obtain approximations to the first and second derivatives of variables. On the contrary, finite volume uses the integral form of the conservation equations. The solution domain is subdivided into a finite number of contiguous control volumes. At the centroid of each (cv) lies a computational node at which the variable values are calculated. Interpolation is used to express variable values at the (cv) surface in terms of nodal (cv-center) values. Surface and volume integrals are approximated using suitable quadrature formulae. As a result, one obtains an algebraic equation for each (cv), in which number of neighbor nodal values appear.

3.2 Numerical modeling for circulating fluidized bed conditions

Most studies of circulating fluidized bed flow however are concerned with the Eulerian model to save computation time. This model is able to predict the formation of clusters and time-averaged solid concentration and flux distribution in circulating fluidized beds. In order to get better understanding of cluster formation and behavior, a few of researchers used Lagrangian models for the simulation of the multiphase flow in fluidized beds (Tsuji, Tanaka, Yonemura 1998; Hellad, Ocelli, Tadrist 2000; Wang et al., 2005) [20].

In fluidized systems, the majority of particles form aggregates or clusters, which are regions of high particle concentration as compared to the mean solid concentration in the riser. Horio and Clift (1992) distinguished agglomerates and clusters in the following way: an agglomerate consists of a group of particles held together by inherent inter-particle forces (Van der Waals forces, liquid bridge forces,...), and a cluster is a group of particles held together as a result of hydrodynamic effects. The study of clusters has received a great deal of attention during the last decades resulting in a large number of experimental and numerical works. [21]

Wilhelm and Kwauk (1948) were among the first to produce experimental evidence of particle clusters in fluidized beds. Kaye and Boardman (1962) performed later an interesting study of cluster formation in dilute suspensions. These findings produced considerable discussion, as reported in the (Symp. Interaction between Fluids and Particles) proceedings of 1962. Jayaweera et al. (1964) proposed that clusters comprised of 2–6 spheres fall faster than a single sphere ($10^{-4} < \text{Re}_p < 10$). They found that, in a viscous fluid, 2–6 particles organized themselves in stable cluster configurations falling faster than isolated particles. The rate of fall was found to increase as the average inter-particle distance decreased, in the range of 10–5 dp. When the number of particles surpassed 6, the clusters split and formed stable sub-groups of clusters. Other researchers (Fortes et al., 1987) have observed similar findings in configurations with far higher Reynolds particle numbers (up to 1800). They observed the drafting (sucking of particles into the wake region of another particles), and kissing

and tumbling in liquid–solid beds. Gunn and Malik (1967) found that, in regions containing few particles distributed non-uniformly, the descent of a given particle can create a velocity field throughout the fluid which tends to decrease the drag of all nearby particles due to the bypassing of the return flow. Yerushalmi et al. (1976) measured large slip velocities in fast fluidized beds, which later were attributed to the formation of clusters (Matsen, 1982). Matsen (1982) stated that for very dilute system $\varepsilon > 0.9997$, the effective drag is that of an isolated particle. He further remarked that with increased loading, the effective drag decreased to a minimum value of approximately $\varepsilon = 0.98$. As the loading further increased, the effective drag began to increase, eventually surpassing the drag of an isolated particle. Other cluster investigations include the work of Grace and Tuot (1979), which proposes an origin of clusters based on Jackson’s stability analysis. Chen et al. (1991) conducted a similarity analysis to study the hydrodynamics of a multi-particle suspended system and to highlight the similarities between cluster formation in gas–solid and liquid –solid systems. Horio and Kuroki (1994), as well as Van Den Moortel et al. (1998) carried out flow visualisations of heterogeneous structures of particles and cluster size/solid velocity measurements in circulating fluidized beds. Sharma et al. (2000) investigated the effect of particle size and superficial velocity on the duration time, occurrence frequency, time-fraction of existence and solid concentration of clusters using capacitance-probe measurements of instantaneous local solid concentration in a fast-fluidized bed. These results were later used to validate the numerical approach used in this study (Helland et al., 2002). The numerical investigation of cluster formation in fluidized beds was first conducted by Tsuo and Gidaspow (1990), based on a two-fluid model (Eulerian/Eulerian simulations). They investigated the effects of gas velocity, solid flow rate, particle size and pipe diameter on cluster formation in a fluidized bed. O’Brien and Syamlal (1991) performed numerical studies in which they included a cluster effect correction of the drag in order to correctly predict the average pressure drop in a circulating fluidized bed. Hoomans et al. (1998) conducted Eulerian/Lagrangian simulations indicating that inelastic collisions enhance cluster growth. Tsuji et al. (1998) compared the cluster patterns determined based on a discrete particle model and that based on a two-fluid model. Ito et al. (1998) carried out a discrete particle (DSMC) study of cluster behaviour which showed good agreement with flow pattern visualisations. Ouyang and Li (1999) studied the effects of gas velocity, solid flow rate, and inelastic collisions on cluster formation using Euler/Lagrangian simulations. More recently, Helland et al. (2000) as well as Li and Kuipers (2002) studied the influence of the porosity function in the drag law on the heterogeneous structures in gas–particle flows. Different groups have now started to use Direct Numerical Simulations (DNS) to further investigate multi-particle systems (Wachmann et al., 1998; Pan et al., 2002; Joseph, 2002). Wachmann et al. showed that the numerical results from DNS match the experimental Richardson and Zaki (1954) correlation determined by a series of studies. [21]

Segregation of particles is an important phenomenon in different industries. Particles of different size have different effects on the flow behavior. To shed some light on these

effects, most researchers started of by investigating binary mixtures. Jenkins and Mancini (1987) extended the kinetic theory for granular flow with corrections of the granular temperature for the individual phases. Gidaspow et al. (1996) and Manger (1996) extended the kinetic theory to binary solids mixtures applying a separate granular temperature for each particle phase. Applying the latter model, Mathiesen et al (1999, 2000) studied the particle dynamics of binary mixtures with various sizes in a riser. Lu & Gidaspow (2003) used a similar model to study binary granular mixtures. Lagrangian model, an arbitrary particle size or density distribution can be used, because the physical properties can be defined for each individual particle. Lagrangian models are more straightforward to apply for studying the flow with binary particle mixtures, since it is relatively easy to obtain the behavior of different particle phases and the distribution and segregation of particles. For this reason, this method is becoming more and more popular to simulate the flow behavior in bidisperse gas-solid fluidized beds.

4 RESULTS AND DISCUSSIONS

4.1 Turbulent Boundary Layer modeling

The behaviour (influence) of the solid phase concentration

The behaviour of particles with high and low phase concentration is different, as shown in Figs. 6 – 9. It is known that the increase of the particle mass concentration as well as decrease of the particle size results in decrease of the velocity slip between average velocities of gas and dispersed phases [10], which is indirectly expressed via the profiles of the radial velocity component of the dispersed phase obtained at the motion of relatively small particles of 25 μm at the high flow mass ratio (bold solid line, Fig. 8) versus distribution of the same velocity at low mass ratio (solid line, Fig. 8). The effect of the mass ratio is mostly pronounced in the profile of the turbulent energy as the low level of turbulence at the high flow mass ratio (solid bold line, Fig. 7) versus the higher level of turbulence at low mass loading (solid line, Fig. 7), which is called as the turbulence modulation caused by the presence of the particles. The small changes of x-velocity and the mass concentration profiles can be seen in Figs. 6 and 9, respectively, for various flow mass ratios.

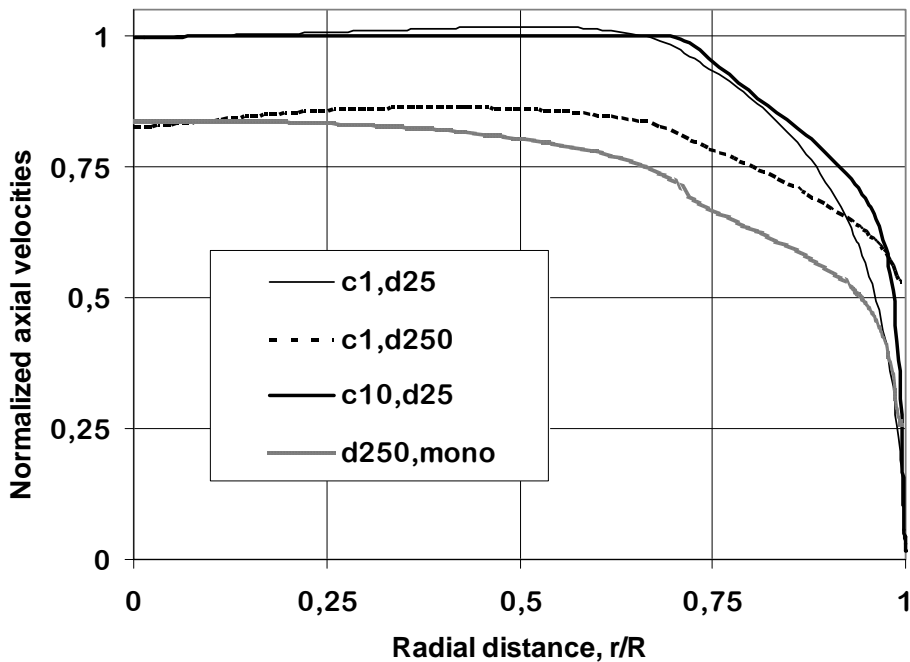


Figure 6. x-velocity profiles of dispersed phase for different particle sizes and mass ratios

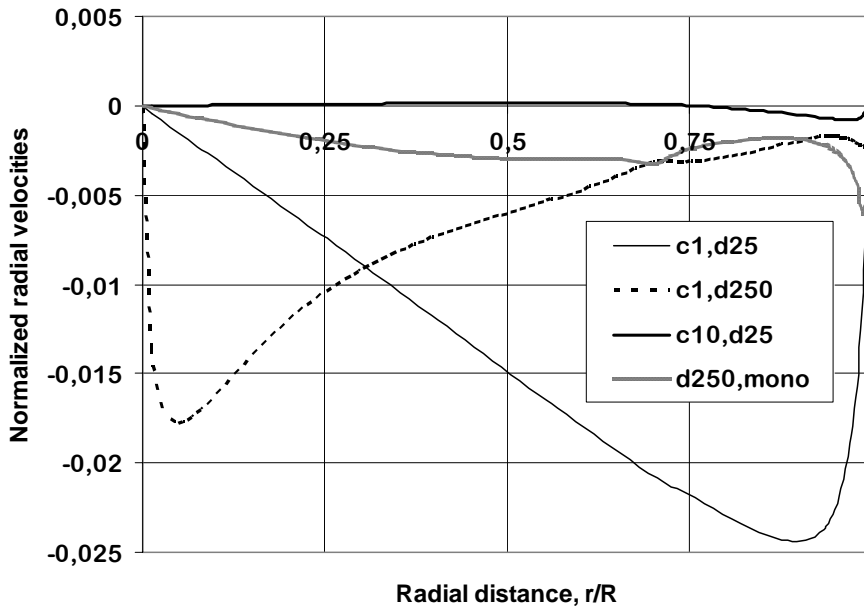


Figure 7. Radial velocity profiles of particles for different particle sizes and mass ratios

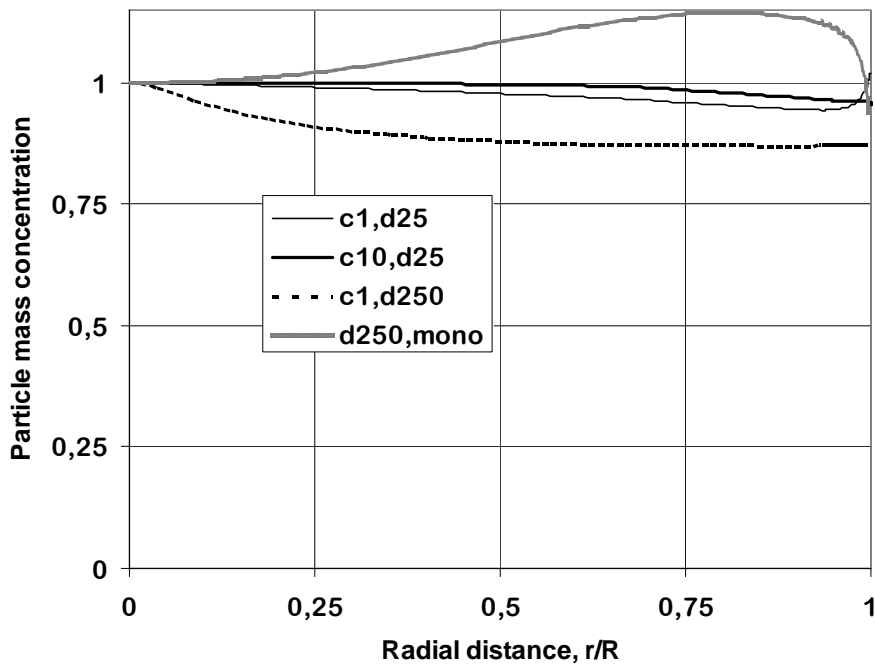


Figure 8. Profiles of particle mass concentration for different particle sizes and mass ratio

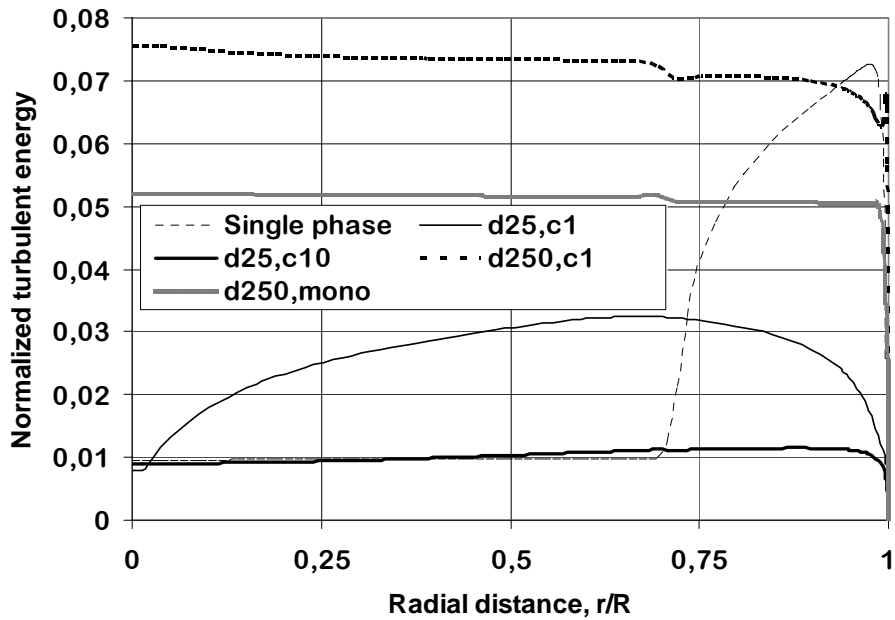


Figure 9. *r.m.s.* profiles of turbulent energy for different particle sizes and mass ratios

The influence of the particle size

This obvious effect is expressed by the distribution of the particles velocity component toward x-axis obtained at the same mass ratio of 1 kg dust/kg air for relatively small 25 μm and coarse 250 μm particles (Fig. 6), namely, the smaller particles have the higher level (solid line) that those of the larger ones (bold dotted line). With respect of the distribution of the radial velocity component, the small particles have the higher velocity in the vicinity of the wall (solid line, Fig. 7) in contrast to the velocity growth occurred close to the axis in case of a motion of the large particles (bold solid line, Fig. 7). This is due to the stronger Magnus effect of the lift force causing the lag motion of the large particles shifting them towards the axis. The manifest effect of the particle size can be seen from the distribution of the turbulent energy, namely, the larger particles generate the higher additional turbulent energy due to the vortex shedding than those of the small ones (cf. bold dotted line and solid line Fig. 9). The mass profiles of the small and coarse particles are slightly different, i.e. the concentration of the small particles has the less gradient as compared to the coarse particles (cf. bold dotted line for large and solid line for small particles, Fig. 8).

The inter-particle collisions

The effect of the inter-particle collisions is important for the particulate flows of the mass ratio larger than 1 kg dust/kg air, when $\tau_c/\tau_p < 1$, where the time of interparticle collision τ_c is less than the particle response time τ_p . We ran the calculations taking into

account the inter-particle collisions described by the pseudoviscosity coefficients (Eq. (2.7)), using the original model of closure based on the particle collisions [7]. To show an importance of this effect one set of the calculations was performed neglecting the particles collisions (cf. bold dotted and pale lines, Fig. 6) in case of motion of the rough 250 μm particles while comparing x-velocity profiles of the dispersed phase with mass ratio of 10 kg dust/kg air. The change of these profiles is obvious, namely, in case of no collision the x-velocity profile becomes narrower that is evidently linked with a reduction of the particles diffusion in the radial direction caused by the inter-particle collisions [7,12]. Besides, the collision effect results in additional turbulence generation derived from the four-way coupling model of Crowe & Gillandts [11] (cf. bold dotted and pale lines, Fig. 9).

The distribution of the radial velocity of the dispersed phase shows that the absence of collisions diminishes the Magnus lift force due to the less velocity slip and therefore the less value of the radial velocity of particles (cf. bold dotted and pale lines, Fig. 7). Finally, the neglect of collisions leads to a growth of concentration in the wall vicinity (cf. pale line versus bold dotted line, Fig. 8), because of underestimating of diffusion of particles.

As a whole, the inter-particle collisions generate the high turbulence and, thus, contribute to the better particle mixing.

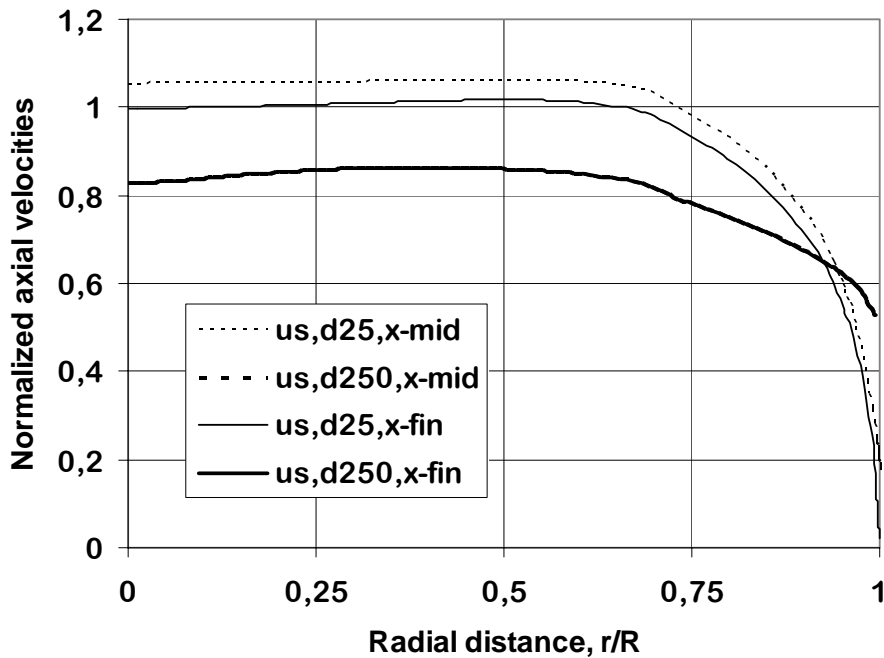


Figure 10. Progress of x-particle velocity profiles along the height with collision effect

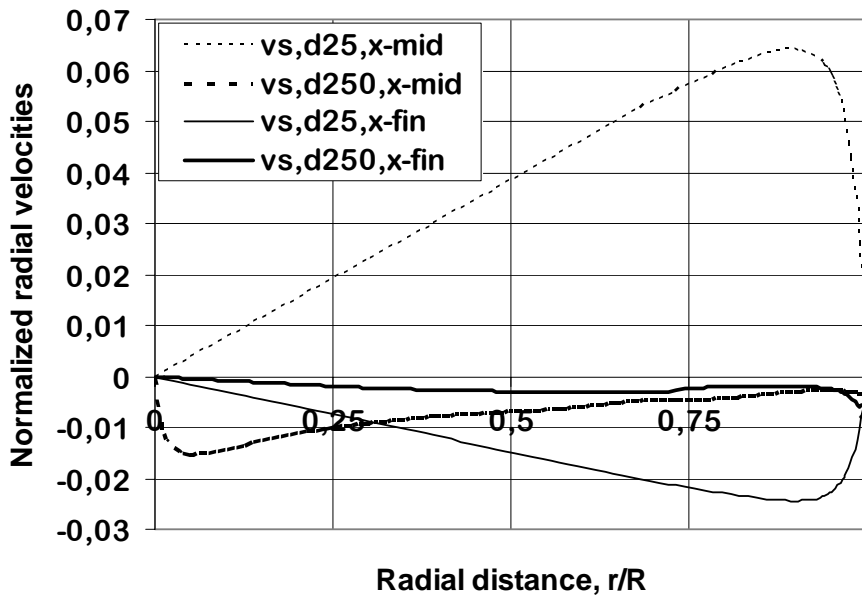


Figure 11. Progress of y particle velocity along the height with collision effect

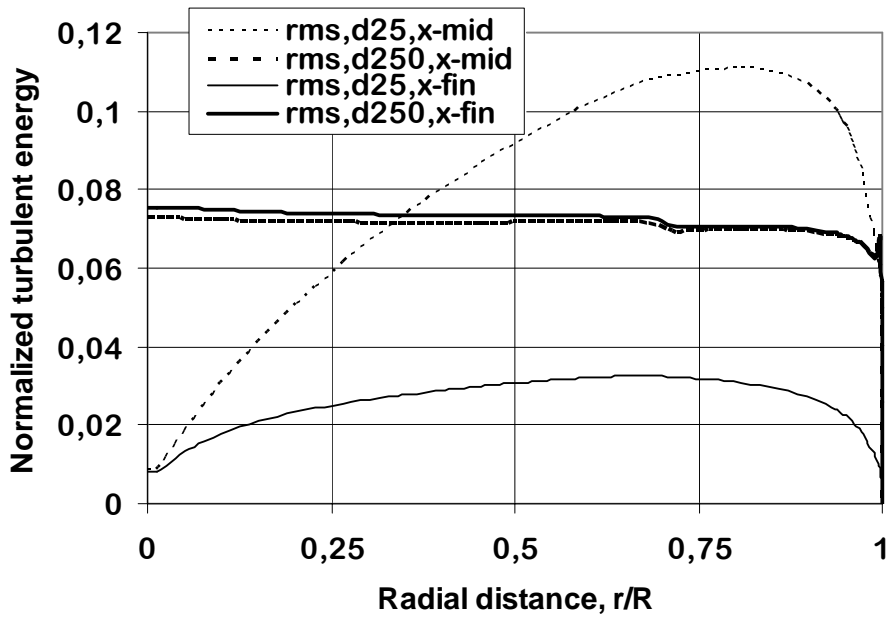


Figure 12. Progress of $r.m.s$ velocity along the height with collision effect

Development of upward motion of particles in the vertical riser

In order to follow the two-phase flow development, we started the calculations from the uniform distribution of parameters of the dispersed phase, namely velocity and concentration, set in the initial cross-section and continued them up to the exit cross-section (the whole length was equalled 6 calibres of the riser). Figs.10 – 12 show the results obtained in the middle cross-section (dotted and bold dotted lines) and in the outlet cross-section (solid and bold solid lines) for small 25 μm and coarse 250 μm particles. One can see that the small particles have the high rate of acceleration with the distinct difference of the velocity distribution along the x-axis along the length of the riser contrary to the motion of the coarse particles that are characterized by slightly differing velocity distributions due to short length (6 calibres) and high inertia of particles (cf. bold solid and bold dotted lines, Fig. 10). With respect to the radial velocity component which is responsible for the momentum exchange one can notice the higher value of the velocity in the middle cross-section (dotted line) as compared with the lower value of this velocity at the exit cross-section (solid line), and such change in the velocity is observed in case of motion of the coarse 250 μm particles (cf. bold dotted and bold solid, Fig. 11). This is due to the gradual adjusting of motion of the dispersed phase to the flow conditions of the gas phase, however this is the coupling process. Finally normalised root mean square (r.m.s.) velocity of the gas phase is fitted to the flow conditions downstream, so the small particles reduce the initial high level of turbulence due to artificial set as uniform velocity distribution in the inlet cross-section (cf. profiles with dotted line and solid line, Fig. 12) and in case of motion of the coarse particles the turbulent energy in terms of the r.m.s distribution slightly changes from the middle to the outlet cross-section (cf. bold dotted and bold solid lines, Fig. 12).

Thus, the parameters of the dispersed phase artificially set in the inlet cross-section are modified to fit the flow conditions downstream.

4.2 2-Dimensional Reynolds Averaged Navier-Stokes modeling

In the RANS computations the *control volume* method was used. The governing equations (p 2.2.2.) were solved using the ILU method, which incorporates a strong implicit procedure with lower and upper matrix decomposition and with an up-wind scheme. For the computations presented in this paper, 600000 uniformly sized volumes were used. The wall functions, obtained from Peric and Scheuerer (1989) were incorporated at a dimensionless distance $y^+=11$ from the wall. All computations were extended from the pipe entrance to a distance $x/D=30$. For the particulate phases, where the size of particles is often larger than the size of the viscous boundary sublayer, we employed the numerical method developed by Hussainov [10] and used wall functions to set gas-phase axial velocity and turbulent energy required for 2D RANS approach. All results are presented in dimensionless way: the velocities of both phases are related to gas-phase velocity at center of flow ($r=0$), the turbulent energy –

to square of gas-phase velocity at flow center, the particle mass concentration – to its value at flow domain center ($r=0$).

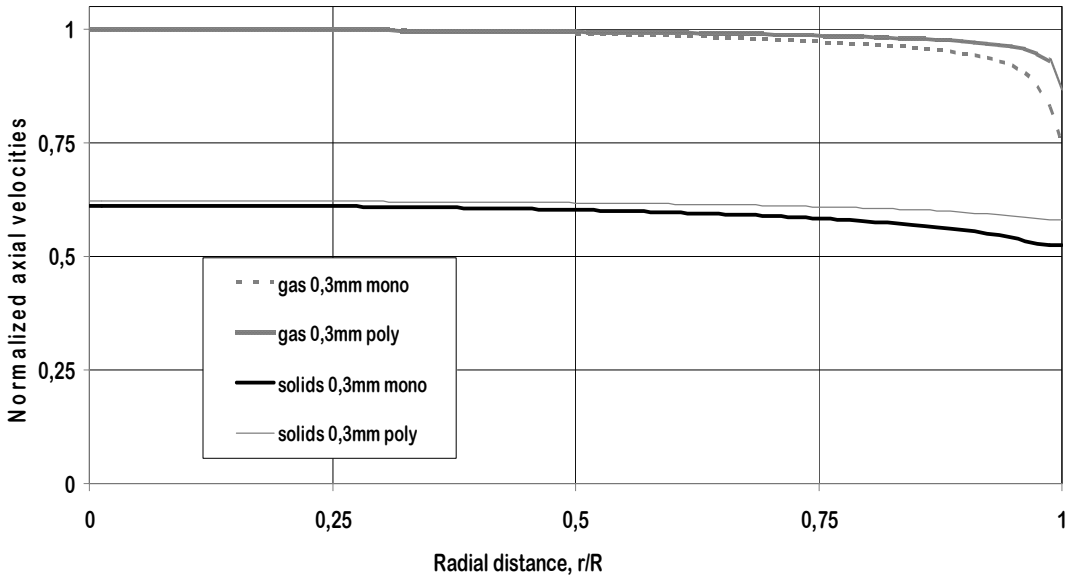


Figure 13. Axial velocity distribution of gas- and dispersed phases for particles (0,3mm) with and without collision effect

The results of the simulation are shown at figures. In fig. 13 there is axial velocity of carrier fluid (gas-phase) and dispersed phase in case of solid particles of diameter 0.3 mm, calculated for different flow conditions – with and w/o particle collisions. As one can noticed the particle collision results in alignment of velocity profiles of dispersed phase. In polydispersed case it is observed smaller velocity slip between gas-phase and average velocity of dispersed phase over three particle fractions. This is due to presence of smaller particle traction among other “mean” and large particle fractions in polydispersed phase composition which is versus the case of monofraction particle fractions composition with the same particle sizes. Eventually it produces large drag than that of polydispersed sold phase motion.

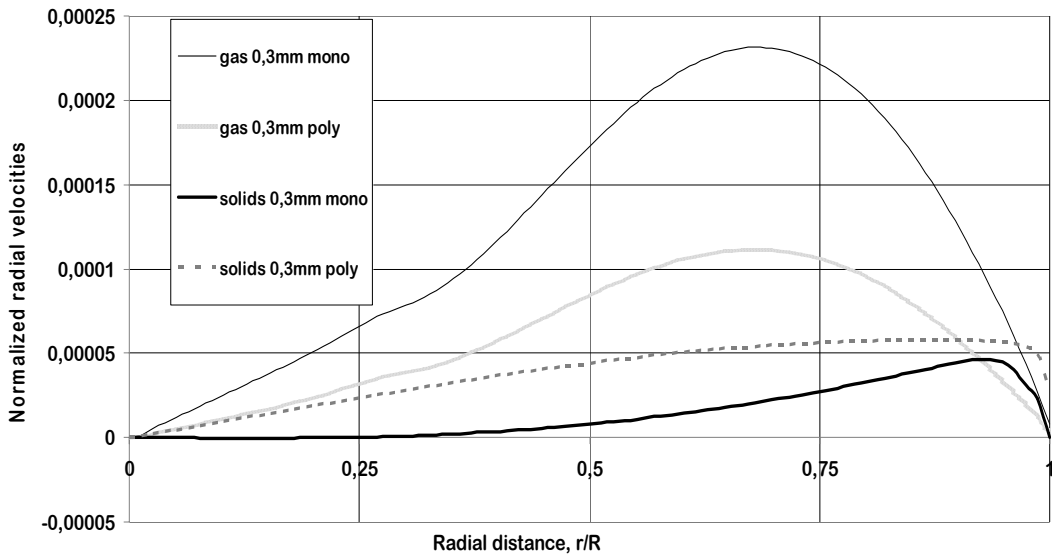


Figure 14. Radial velocity profiles of gas- and dispersed phases for particles (0,3mm) with and without collision effect

Fig.14 shows that radial velocity of both phases which increases off axis and has highest magnitude somewhere in a middle of the flow cross-section. This indicates that radial velocity in case of two-phase flow is not negligible in comparison with axial velocity component like in single-phase turbulent pipe flow and it is formed by lift Magnus and Saffman forces along its redistribution owing to effect of particle collisions in the dispersed phase. As a result it redistributes and forms the particle mass concentration in flow cross-sections. In both cases at the motion of monodispersed and polydispersed particles (collision motion) it should take into account an important role of radial velocity of dispersed phase. The effect of particle collisions levels the radial velocity of dispersed phases.

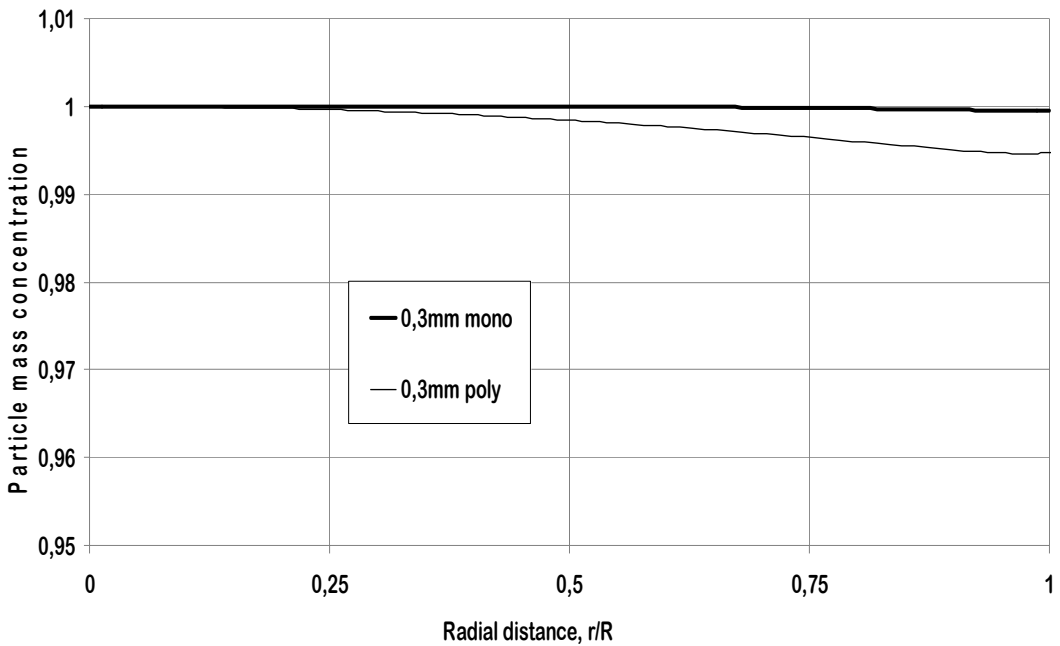


Figure 15. Mass concentration distribution for particles (0,3mm) with and without collision effect

The figure 15 shows the distribution of the mass concentration for small particles (0.3 mm) with and without particle collisions. The profiles of particle mass concentration are almost flat with slightly decreases of distribution of mass concentration towards the wall in case of polydispersed phase. In this case the coefficient turbulent diffusion of particles is sufficiently large to make uniform the particle's mass distribution across the flow.

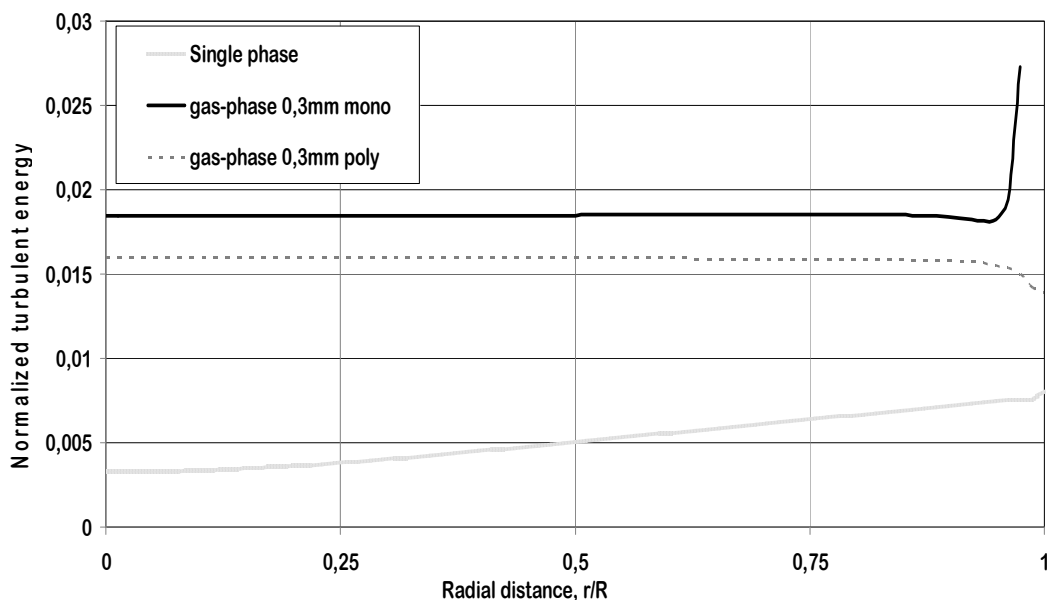


Figure 16. Turbulent energy profiles of single and gas phases for particles (0,3mm) with and without collision effect

The fig. 16 shows distribution of turbulence at the motion of relatively small solid particles of 0.3 mm for two regimes - with and without particle collisions. One can indicate that the presence of particles leads to turbulence enhancement in turbulent core and in the wall vicinity in comparison with case of single-phase flow. It follows from four-way coupling model [11] by introducing square of velocity lag between gas- and dispersed phases (last term in right-hand side of equation 2.12 in p.2.2.2.) which is responsible for additional turbulence generation. The physics behind this is formation of vortex shedding generated from streamlined inertia large solid particles. This process is less pronounced for polydispersed phase with lower level additional turbulence generation than for monodispersed phase because of smaller velocity slip occurred at the motion of polydispersed phase (fig. 13).

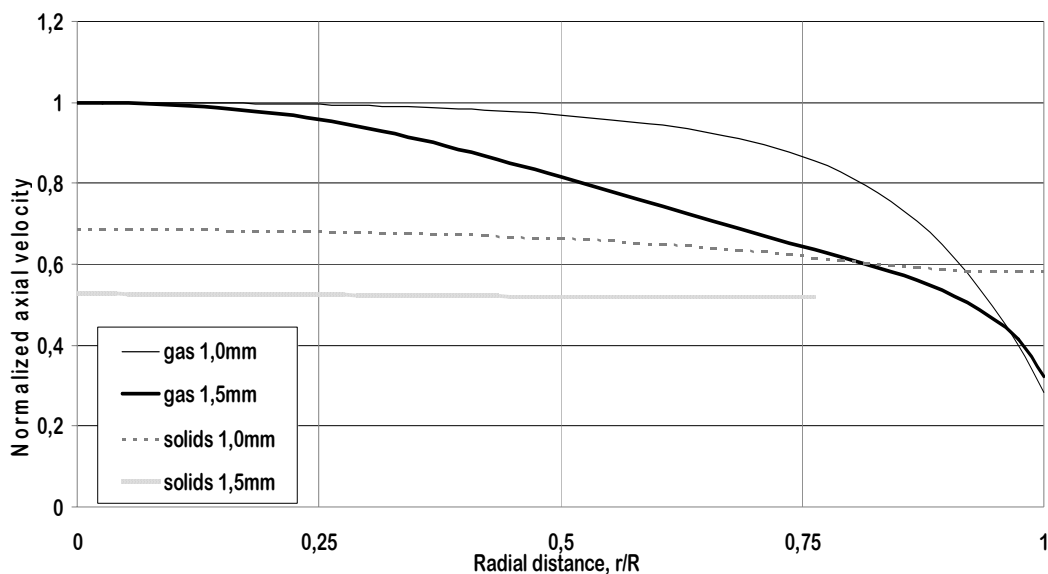


Figure 17. Axial velocity profiles of gas- and dispersed phases for different particle sizes (1,0 and 1,5 mm)

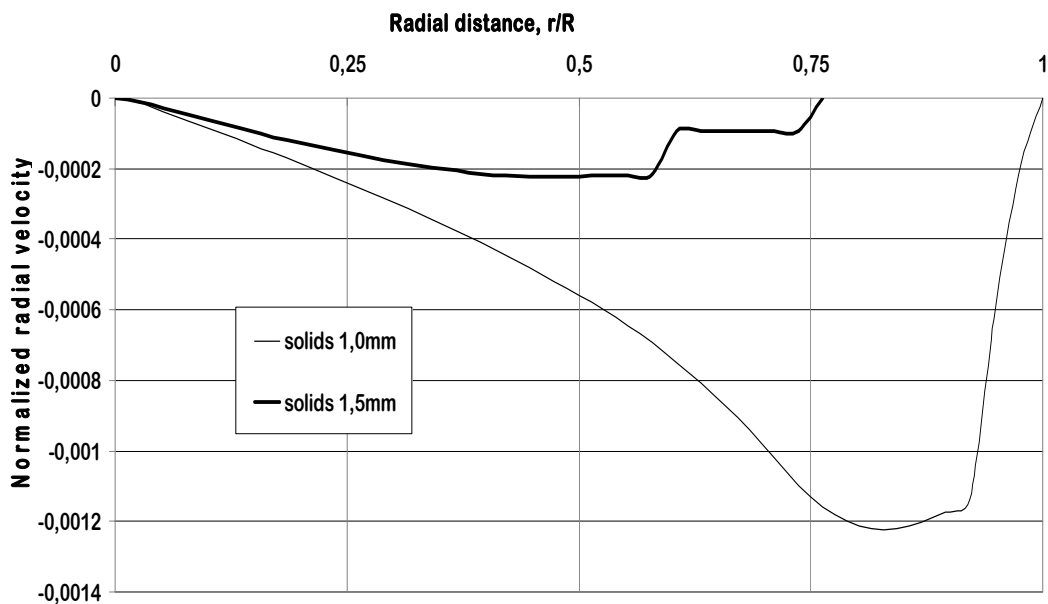


Figure 18. Radial velocity profiles for different particle sizes (1,0 and 1,5 mm)

The following case with larger particle sizes of 1 and 1.5 mm shows increase of velocity slip between phases versus previous case with smaller sizes of particles and it

is observed both in axial radial directions (figs. 17 and 18). So, the mathematical model gives reasonable results of profiles of flow parameters (averaged velocities of gas- and dispersed phases, turbulent energy).

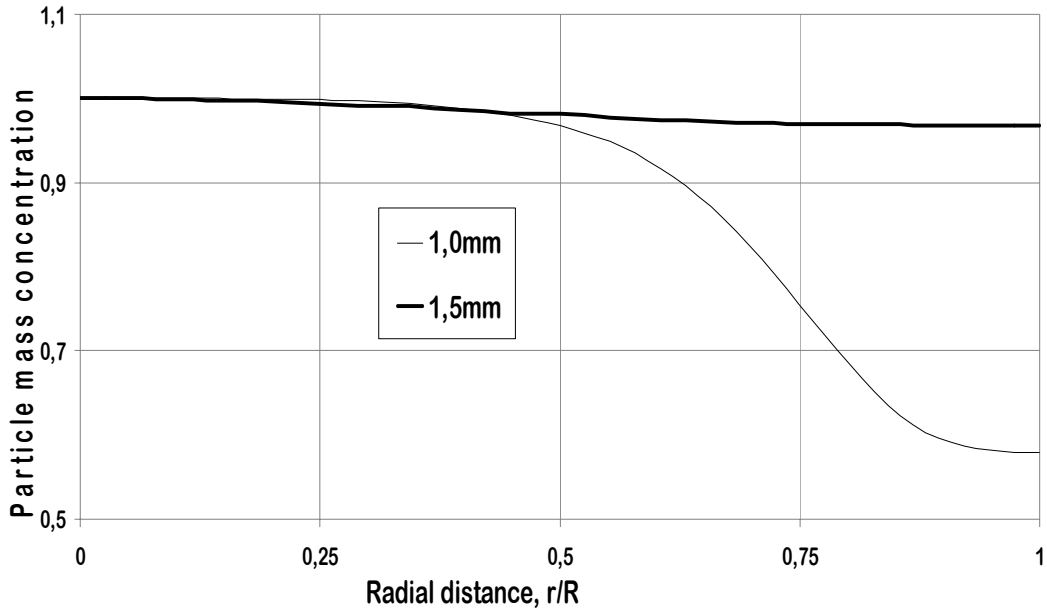


Figure 19. Mass concentration distribution for different particle sizes (1,0 and 1,5 mm)

The presence of large particles of 1 and 1.5 mm may noticeable effect on turbulence redistribution causing growth turbulence for motion of larger particles of 1.5 mm (fig. 20). It comes from higher velocity lag for such particles versus particles of 1 mm.

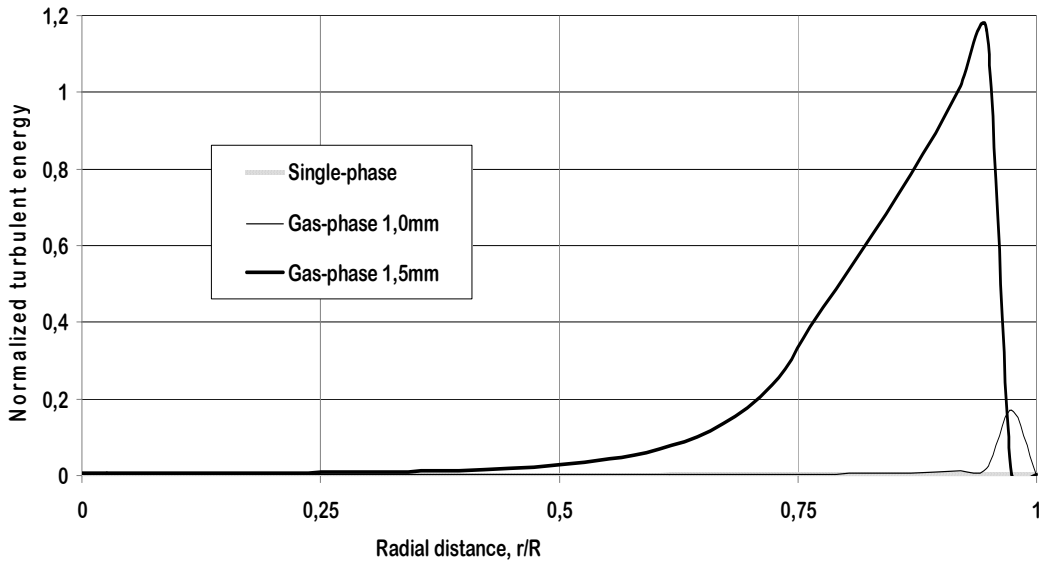


Figure 20. Turbulent energy profiles of single and gas phases for different particle sizes (1,0 and 1,5 mm)

Figure 20 shows two k-profiles (turbulent energy) at the motion of relatively large particles, of 1 and 1.5 mm.

In case of larger particles, of 1.5mm one can see jump in distributions of axial (fig. 17) and radial velocity of solids (fig. 13) together with particle mass concentration (fig. 19). The jump in distributions of radial velocity of solids and the particle mass concentration in vicinity of the wall is analyzed in [7]. It's stemmed from finite size of such rough particles which is comparable or larger of mesh size of numerical grid. Due to comparable size of such rough particles they may occupy smaller flow domain focusing on vicinity of the wall where gas-phase may less effect of their motion and mainly they fall down along the walls. Therefore in order to keep moving such rough particles upward flow it should be some value of flow velocity holding there versus gravitation. We determined flow the region where such rough of 1.5 mm particles move upward flow.

The high level of additional turbulent energy production by rough particles is result of high velocity slip in a turbulent core of the flow as well as substantial velocity slip in wall region. In both given cases of 1 and 1.5 mm, the presence of such rough solid particles results in turbulence enhancement versus single-phase flow.

The distribution of mass concentration is shown in figure 15 for different particle sizes (1 and 1.5 mm). The mass concentration of the particles depends on their radial velocity show in fig. 18.

Compare of the results

Comparing the results of two different modulations, we can notice next remarkable facts:

- The 2D RANS approach gives more comprehensive picture of description of phenomena in CFB versus TBL (turbulent boundary layer approach) with respect distribution of average velocity components of both phases the turbulent energy and particle mass concentration. The inter-particle collision in considered RANS method results in redistribution of velocities, turbulent energy and mass concentration not only in radial direction but in streamwise direction as well. The numerical results obtained for two cases with and w/o particle collision qualitatively are close and different quantitatively underlining that in conditions of CFB operating with dense particle flow the effect of particle collision indispensably have taken into account.
- The particle mass concentration in 2D RANS results is bigger, comparing coarse particles to the smaller ones. It is caused by the big turbulence diffusion in the vicinity of the wall. Also to make certain conclusions in particle mass concentration, the flow has to be fully developed, but our one is not.

CONCLUSIONS

The work performs numerical simulation of CFB process by two approaches TBL (Turbulent Boundary Layer) and 2D RANS (two dimensional Reynolds Average Navier-Stokes) equations using two-fluid (Euler/Euler approximation). The numerical results were validated by existed experimental data.

The both TBL and 2D RANS approaches were performed in conditions of non-isothermal conditions of CFB (about 800⁰ C) with respect of higher value of kinematic viscosity of carrier (gas-phase) flow and lower value of its density versus these parameters for normal conditions.

The processes in fluidized bed dealt with noticeable mass loading of the flow where the dispersed phase, that is heat carrier, was modelled by ash solid particles with particles size distribution. The both approaches, the TBL and 2D RANS methods showed

- i) key role of turbulence enhancement due to substantial velocity slip between the carrier gas-phase flow and the dispersed phase, heat carrier which generates additional turbulence by particle's vortex shedding; the TBL approach a bit overestimates turbulences enhancement (turbulence exceed above turbulence level in single phase flow) versus results from 2D RANS approach.
- ii) at the same time importance of inter-particle collisions which contributes to increase of turbulence generation and also resulting in redistribution of particle mass concentration in CFB flow domain.
- iii) the turbulence enhancement is the desired effect to intensifying mixture process in combustion stage in CFB.

The modeling CFB processes by TBL performed in laboratory conditions with extension of the modeling into simulation of real CFB process occurred for real ash particle fractions and real geometry flow domain showed that presented mathematical description capture adequately thermodynamic processes occurred in real performance of CFB.

REFERENCES

1. Arro, H., Pihu, T., Prikk, A., Rootamm, R., Konist, A., 2009, Comparison of ash from PF and CFB boilers and behavior of ash in ash fields. *Proceedings of the 20th International Conference on Fluidized Bed Combustion*, no. 2, pp. 1054–1060.
2. Andrews IV, Arthur T., 2007, Filtered models for gas-particle flow hydrodynamics.
3. Cao, J., Ahmadi, G., 1995, Gas-particle two-phase turbulent flow in vertical duct, I *International Journal of Multiphase Flows*, vol. 21, pp. 1203–1228.
4. Chen, Y.-M., Jang, C.-S., Cai, P., Fan, L.-S., 1991, On the formation and disintegration of particle clusters in a liquid–solid transport bed. *Chemical Engineering Science*, vol. 46 (9), pp. 2253–2268.
5. Clift, R., Grace, J.R., Weber, M.E. 1978, Bubbles, drops and particles. *Academic Press*, New York.
6. Crowe, C.T., Stock, D.E., Sharma, M.P., 1977, The particle-source-in cell PSI-CELL model for gas-droplet flows. *ASME, Transactions, Series I - Journal of Fluids Engineering*, vol. 99, pp. 325–332.
7. Crowe, C. T., Gillandt, I., 1998, Turbulence modulation of fluid-particle flows – a basic approach. *Third ICMF*, Lyon.
8. Crowe, C., Sommerfeld, M., Tsuji, Y., 1998, Multiphase flows for droplets and particles.
9. Crowe C. T., 1993, Modeling Turbulence in Multiphase Flows. *Engineering Turbulence Modeling and Experiments*, vol. 2, pp. 899–913.
10. Crowe C. T., Troutt, T. R., Chung J. N., 1996, Numerical Models for Two-Phase Turbulent Flows. *Ann. Rev. Fluid Mech.*, vol. 28, pp. 11–43.
11. Elgobashi, S., Truesdell, G. C., 1993, On the two-way interaction between homogeneous turbulence and dispersed solid particles. I. *Turbulence Modification. Physics of Fluids*, vol. 5, pp. 1790–1801.
12. Ferziger, J., Peric, M., 1996, Computational Methods for Fluid Dynamics.
13. Fortes, A.F., Joseph, D.D., Lundgren, T.S., 1987, Nonlinear mechanics of fluidization of beds of spherical particles. *Journal of Fluids Mechanics*, vol. 177, pp. 467–483.
14. Frishman, F., Hussainov, M., Kartushinsky, A., Mulgi, A., 1997, Numerical simulation of a two-phase turbulent pipe-jet flow loaded with polyfractional solid admixture. *Int. J. Multiphase Flow*, vol. 23, no. 4, pp. 765–796.
15. Gidaspo, D., 1994, Multiphase Flow and Fluidization. Continuum and Kinetic Theory Description. *Academic Press*, New York.
16. Gore, R., Crowe, C., 1989, Effect of particle size on modulating turbulent intensity. *International Journal of Multiphase Flow*, vol. 15, pp. 279–285.
17. Grace, J.R., Tuot, J., 1979, A theory for cluster formation in vertically conveyed suspensions of intermediate density. *Transactions of Industrial and Chemical Engineering*, vol. 57, pp. 49–54.

18. Gunn, D.J., Malik, A.A., 1967, The structure of fluidized beds in particulate fluidization. *Proceedings of the International Symposium on Fluidization*, Einhoven, pp. 52–65.
19. Happel, M., Brenner, H., 1973, Low Reynolds Number Hydrodynamics: with special applications to particulate media. *Mechanics of Fluids and Transport Processes*.
20. He, Y., Deen, N.G., van Sint Annaland, M., J.A.M. Kuipers, J.A.M., 2008, Gas-solid turbulent flow in a circulating fluidized bed riser; numerical study of binary particles mixtures. *9th International Conference on Circulating Fluidized Beds*, Germany.
21. Helland, E., Occelli, R., Tradist, L., 2000, Numerical study of cluster formation in a gas-particle circulating fluidized bed. *Powder Technology*, vol. 100, pp. 210–221.
22. Helland, E., Occelli, R., Tadriss, L., 2002. Computational study of fluctuating motions and cluster structures in gas-particle flows. *International Journal of Multiphase Flows*, vol. 28/2, pp. 199–223.
23. Hestroni, G., 1989, Particles-turbulent interaction. *International Journal of Multiphase Flow*, vol. 15, pp. 735–747.
24. Hoomans, B.P.B., Kuipers, J.A.M., Van Swaaij, W.P.M., 1998, Granular dynamics simulation of cluster formation in dense riser flow. *Third International Conference on Multiphase Flow*, Lyon, France, pp. 2.7–9.
25. Horio, M., Clift, R., 1992, A note on terminology: “clusters” and “agglomerates”. *Powder Technology*, vol. 70, p. 196.
26. Horio, M., Kuroki, H., 1994, Three-dimensional flow visualization of dilutely dispersed solids in bubbling and circulating fluidized beds. *Chemical Engineering Science*, vol. 49 (15), pp. 2413–2421.
27. Hussain, A., Ani, F. N., Darus, A. N., Mustafa, A., Salema, A. A., Proceedings of the 18th International Conference on Fluidized Bed Combustion, *ASME Publication*, 2005. p. 1–7.
28. Hussainov, M., Kartushinsky, A., Mulgi, A., Rudi, Ü., Tisler, S., 1995, Experimental and Theoretical Study of the Distribution of Mass Concentration of Solid Particles in the Two-Phase Laminar Boundary Layer on a Flat Plate, *International Journal of Multiphase Flow*, vol. 21, no. 6, pp. 1141–1161.
29. Hussainov, M., Kartushinsky, A., Mulgi, A., Rudi, Ü., 1996, Gas-solid flow with the slip velocity of particles in a horizontal channel. *J. Aerosol Science*, vol. 27, no. 1, pp. 41–59.
30. Hussainov, M., 2005. Effect of Solid Particles on Turbulence of Gas in Two-Phase Flows. Ph.D. thesis, Tallinn University of Technology.
31. Ito, M., Tsukada, M., Shinamura, J., Horio, M., 1998, Prediction of cluster size and slip velocity in circulating fluidized beds by a DSMC model. *Fluidization IX*, Durango, USA, pp. 525–532.
32. Jayaweera, K.O.L.F., Mason, B.J., Slack, G.W., 1964, The behaviour of clusters of spheres falling in a viscous fluid. Part I. *Experiment. Journal of Fluid Mechanics*, vol. 20, pp. 121–128.

33. Jenkins J.T., Mancini F., 1989, Kinetic theory for binary mixtures of smooth, nearly elastic spheres. *Physics of Fluids*, vol. 31, pp. 2050–2057.
34. Joseph, D.D., 2002, Interrogations of direct numerical simulation of solid–liquid flow, University of Minnesota.
<http://www.efluids.com/efluids/books/joseph.htm>.
35. Kartushinsky, A., Michaelides, E., 2004, An analytical approach for the closure equations of gas-solid flows with inter-particle collisions. *International Journal of Multiphase Flow*, vol. 30, pp. 159–180.
36. Kartushinsky, A., Michaelides, E. E., 2006, Particle-laden gas flow in horizontal channels with collision effects. *Powder Technology*, vol. 168, pp. 89–103.
37. Kartushinsky, A., Michaelides, E. E., 2007, Gas-solid particle flow in horizontal channel: decomposition of the particle-phase flow and inter-particle collision effect. *Journal of Fluids Engineering, the Transaction of ASME*, vol. 129, no. 6, pp. 702–712.
38. Kavidass, S. Szumania, M. J., Alexander, K. C., 1996, Design conditions of Babcock & Wilcox industrial and utility size reheat/non-reheat IR-CFB boilers. *POWER-Gen Asia '96 Exhibition & Conference*, New Delhi, India, 12p.
39. Kaye, B.H., Boardman, R.P., 1962, Cluster formation in dilute suspensions. *Proceedings of the Symposium on Interaction between Fluids and Particles*, British Institute of Chemical Engineers, London, pp. 17–21.
40. Kenning, V., Crowe, C., 1996, Brief communication on the effect of particles on carrier phase turbulence in gas-particles flow.
41. Kunii, D., Levenspiel, O., 1991, Fluid Engineering. Butterworth Heinemann series in Chemical Engineering, London, UK.
42. Li, J., Kuipers, J.A.M., 2002, Flow structure formation in high velocity gas-fluidized beds. *Fluidization X*, Beijing, China.
43. Louge, M.Y., Mastorakos, E., Jenkins, J.T., 1991, The role of particle collisions in pneumatic transport, *Journal of Fluid Mechanics*, vol. 231, pp. 345–359.
44. Manger, E., 1996, Modeling and simulation of gas/solid flow in curvilinear coordinates. Ph.D. thesis, Telemark Institute of Technology, Norway.
45. Marble, F.E., 1964, Mechanism of particle collision in one-dimensional dynamics of gas-particle admixture, *Phys. Fluids*, vol. 7, pp. 1270–1282.
46. Mathiesen, V., Solberg, T., Arastoopour, H., Hjertager, B.H., 1999, Experimental and computational study of multiphase gas/particle flow in a CFB riser. *A.I.Ch.E. Journal*, vol. 45, pp. 2503–2518.
47. Mathiesen, V., Solberg, T., Hjertager, B.H., 2000, An experimental and computational study of multiphase flow behavior in a circulating fluidized bed. *International Journal of Multiphase Flow*, 26, pp. 387–419.
48. Matsen, J.M., 1982, Mechanisms of choking and entrainment. *Powder Technology*, vol. 32, pp. 21–33.

49. Munson, B., Young, D., Okiishi, T., 1998, Fundamentals of fluid mechanics, 877p.
50. O'Brien, T.J., Syamlal, M., 1991. In: Gaden, E.L., Weimer, A.W. (Eds.), Advances in Fluidized Systems, *A.I.Ch.E. Symposium Services*, vol. 281(87), pp. 127–136.
51. Oesterle, B., Petitjean, A., 1993, Simulation of particle to particle interactions in gas–solid flows, *International Journal of Multiphase Flows*, vol. 19, pp. 199–211.
52. Oil shale perspectives within energy production, Estonia. Outline proposal for 100 MWth demonstration CFB boiler. Lurgi Energie und Umwelt GmbH, Frankfurt am Main, 1995, 25p.
53. Ots, A., 2006, Oil Shale Fuel Combustion, 883p.
54. Ouyang, J., Li, J., 1999, Discrete simulations of heterogeneous structure and dynamic behavior in gas–solidfluid ization. *Chemical Engineering Sciences*, vol. 54, pp. 5427–5440.
55. Pan, T.W., Joseph, D.D., Bai, R., Glowinski, R., Sarin, V., 2002, Fluidization of 1204 spheres: simulation and experiment. *Journal of Fluid Mechanics*, vol. 451, pp. 169–191.
56. Peric, M., Scheuerer, G., Obi, S., 1989, A finite volume calculation procedure for turbulent flows with second-order closure and collocated variable arrangement. *7th Symposium on Turbulent Shear Flows*, Stanford Univeristy.
57. Richardson, J.F., Zaki, W.N., 1954, Sedimentation and fluidization: Part 1. *Transactions of Institute of Chemical Engineers*, vol. 32, pp. 35–53.
58. Sharma, A.K., Tuzla, K., Matsen, J., Chen, J.C., 2000, Parametric effects of particle size and gas velocity on cluster characteristics in fast fluidized beds. *Powder Technology*, vol. 111, pp. 114–122.
59. Shraiber, A., Gavin, L., Naumov, V., Jatsenko, V., 1987, Gas mixture turbulent flows, 240p. [In Russian].
60. Simonin, O., Deutsch, E., Minier, J.-P., 1993, Eulerian prediction of the fluidparticle correlated motion in turbulent two-phase flows, *Appl. Sci. Res.*, vol. 51, pp. 275–283.
61. Simonin, O., 2001, Statistical and continuum modeling of turbulent reactive particulate flows—part i: theoretical derivation of dispersed phase eulerian modeling from probability density function kinetic equation, in: J.-M. Buchlin (Ed.), Von Karman Institute Lecture Series, Brussels, Belgium.
62. Sommerfeld, M., Zivkovic, G. 1992, Recent advances in the numerical simulation of pneumatic conveying through pipe systems, *Comp. Meth. Appl. Sci. Elsevier Sci. Publ. B.V.*, pp. 201–212.
63. Sommerfeld, M., 2003, Analysis of collision effects for turbulent gas-particle flow in a horizontal channel: part I. Particle transport, *International Journal of Multiphase Flows*, vol. 29, pp. 675–699.
64. Squires K. D., Eaton, J. K., 1990, Particle response and turbulence modification in isotropic turbulence. *Physics of Fluids*, A2, pp. 1191–1203.
65. Zhang, W., 1992, Particle flow pattern in circulating fluidized bed boilers.

66. Thermal calculation of power generators (Standard method). Moskva, 1973, 295p. [In Russian].
67. Tisler, S., 2006, Deposition of Solid Particles from Aerosol Flow in Laminar Flat-Plate Boundary Layer. Ph.D. thesis, Tallinn University of Technology.
68. Tsuji, Y., Tanaka, T., Yonemura, S., 1998, *Powder Technology*, vol. 95, pp. 254–264.
69. Tsuo, Y.P., Gidaspow, D., 1990, Computation of flow patterns in circulating fluidized beds. *A.I.Ch.E. Journal*, vol. 36, pp. 885–896.
70. Wachmann, B., Kalthoff, W., Schwarzer, S., Herrmann, H.J., 1998, Collective drag and sedimentation: comparison of simulation and experiment in two and three dimensions. *Granular Matter*, vol. 1, pp. 75–82.
71. Valk, M. (Editor). Atmospheric Fluidized Bed Coal Combustion Research, Development and Application. Amsterdam – Lausanne – New York – Oxford – Shannon – Tokyo, 1995, 462p.
72. van Den Moortel, T., Santini, R., Tadriss, L., Pantaloni, J., 1998, *Fluidisation IX*, Durango, CO, pp. 157–162.
73. van der Hoef, M.A., YeI, M., van Sint Annaland, M., Andrews IV, A.T., Sundaresan S., Kuipers, J.A.M., 2006, Multiscale modeling of gas-fluidized beds. *Advances in Chemical Engineering*, vol. 31
74. van Swaaij, W. P. M., 1985, Chemical reactors. Fluidization *Academic Press*, London, UK (J. F. Davidson, and R. Clift, Eds.).
75. Wang, S., Liu, H., Lu, H., Liu, W., Jiamin, D. and Li, W., 2005, Flow behaviour of clusters in a riser simulated by direct simulation Monte Carlo method. *Chemical Engineering Journal*, vol. 106, pp. 197–211.
76. Wilhelm, R.H., Kwauk, M., 1948, Fluidization of solid particles. *Chemical Engineering Progress*, vol. 44, p. 201.
77. Yamamoto, Y., Potthoff, M., Tanaka, T., Kajishima, T., Tsuji, Y., 2001, Large-eddy simulation of turbulent gas-particle flow in a vertical channel: effect of considering inter-particle collisions, *Journal of Fluid Mechanics*, vol. 442, pp. 303–334.
78. Yerushalmi, J., Tuner, D.H., Squires, A.M., 1976, The fast fluidized bed. *Industrial Engineering Chemical Process Design and Development*, vol. 15, pp. 47–53.
79. Young, D., Munson, B., Okiishki, T., Huebsch, W., 2007, A brief introduction to fluid mechanics.

LIST OF PUBLICATIONS

- I. Kartushinsky, A., Martins, A., Rudi, Ü., Štšeglov, I., Tisler, S., **Krupenski, I.**, Siirde, A. Numerical simulation of uprising gas-solid particles flow in circulating fluidised bed. *Oil-Shale*, 2009, vol.26, no.2, pp. 125–138.
- II. Kartushinsky, A., **Krupenski, I.**, Tisler, S., Hussainov, M., Štšeglov, I. Deposition of solid particles in flat-plate laminar boundary layer. *High temperature thermophysics*, 2009, vol. 47, no.6 pp. 927–936.
- III. **Krupenski, I.**, Kartushinsky, A., Siirde, A., Rudi, Ü. Numerical simulation of uprising gas-solid particle turbulent flow by 2D RANS for fluidized beds conditions. *Oil-Shale* (Accepted for publication).

The personal contribution of the autor

The contribution of the author to the papers included in the thesis is as follows:

- I. Igor Krupenski participated in writing the paper. The author operated with the results of the numerical simulation and worked on the results and discussions.
- II. Igor Krupenski participated in writing the paper. The author worked on the model composition and dealt with the results of the work.
- III. Igor Krupenski is the main author of the paper. He is responsible for the literature overview, analysis, calculation, graphical part and conclusions. He had a major role in writing.

KOKKUVÕTE

Töös käsitletakse tsirkuleeriva keevkihi protsessi matemaatilist modelleerimist kahe meetodiga: TBL (Turbulent Boundary Layer) ja 2D RANS (2-Dimensional Reynolds Averaged Navier-Stokes) võrrandite abil, kasutades nn mudelit „two-fluid” (Euler/Euler ühtlustamine). Modelleerimise tulemused on kinnitatud olemasolevate eksperimentaalsete andmetega.

Mõlema meetodi (TBL ja 2D RANS) modelleerimised olid teostatud tsirkuleeriva keevkihi mitteisotermiliste tingimustega (*ca* 800 °C), arvestades vedava voolu (gaasifaas) kinemaatilise viskoossuse kõrget väärtust ja tiheduse madalat väärtust, võrreldes nende parameetritega normaalsete tingimuste puhul.

Protsessid, mida on uuritud keevkihis, käsitlevad märgatava voolu massi suurenemist, kus dispersne faas, mis on soojuskandja, on modelleeritud tuha tahkete osakestega koos osakeste suuruse jaotusega. Mõlema meetodi (TBL ja 2D RANS) modelleerimised näitasid:

- võtmerolli mängib turbulentsuse suurenemisel kiiruse libisemine vedava voolu (gaasifaas) ja dispersse (soojuskandja) faasi vahel, mis genereerib täiendava turbulentsuse osakeste keerisvoolamisega; TBL meetod veidi ülehindas turbulentsuse suurendamist (turbulentsus ületab turbulentsuse taset ühefaasilise voolu korral), võrreldes tulemustega, mis on saadud 2D RANS meetodi abil;
- samal ajal omavad tähtsust osakestevahelised kokkupõrked, mis genereerivad kõrge turbulentsuse ning mille tulemuseks on ka osakeste masskontsentratsiooni ümberjaotus tsirkuleeriva keevkihi voolu piirkonnas;
- turbulentsuse suurendamine on soovitud eesmärk, mis intensiivistab segunemise protsesse tsirkuleeriva keevkihi põletamise staadiumis.

Tsirkuleeriva keevkihi protsesside modelleerimine TBL meetodiga labori tingimustes, arvestades, et modelleeritakse reaalne tsirkuleeriva keevkihi protsess koos reaalsete tuhaosakeste fraktsioonidega ja reaalse voolu piirkonna geometriaga, näitas, et toodud matemaatiline kirjeldus hõlmab piisavalt termodünaamilise protsessi, mis esineb tsirkuleerivas keevkihis reaalsete omadustega.

ABSTRACT

Estonia is a small country where ca 95% of electricity is produced by oil-shale power plants. Circulating fluidized bed (CFB) technology is installed and launched in 2004 at Estonian Power Plant and at Baltic Power plant where oil-shale is combusted. Since during combusting oil-shale arises a lot of ash, there is no need of using additional material (for example, sand) for solid phase in oil-shale CFB process. In CFB oil-shale ash is circulating.

The concentration of solid particles of the ash and inert material taken place in a combustion chamber of the CFB is very high, that gives a rise to some disadvantages. At the same time, the required temperature level occurred in a combustion chamber is guaranteed by the circulation of solid particles. In this work the numerical simulation of gas-solid particles flow has been performed in a frame of the two-fluid model, namely the Eulerian approach for the dispersed phase, for the conditions of CFB, ranging from moderate to high mass ratios of the flow. An incorporated original model of closure of the transport equations of the dispersed phase permitted to account the interparticle collisions which might be indispensable to proper numerical simulation of process in the considered CFB.

There were performed two numerical simulations using different models: Turbulent Boundary Layer and 2D RANS, which qualitatively and quantitatively describes the real-time distribution of flow parameters in real flow domain, i.e. model covers reasonable physical phenomena occurred in fluidized-beds conditions.

The results of this work would be helpful for improving of the processes occurred in the combustion chamber of CFB.

Keywords: Circulating fluidized bed, CFB numerical simulation, gas-solid particles flow, two-fluid model, 2D RANS.

CURRICULUM VITAE

Name Igor
Surname Krupenski
Date and place of birth 23.06.1983, Estonia
Family status Single
Contact Kadaka pst 169a/a-24, Tallinn, Estonia,
Telephone: +372 58003989;
E-mail: ikrupenski@gmail.com
Workplace K-Projekt AS,
Ahtri 6a, 10151 Tallinn
Appointment Project manager

Education:

Educational institution	Year of graduation	Education
Tallinn University of Technology	2006	Master degree
Tallinn University of Technology	2005	Bachelor degree
Tallinn Tõnismäe Real School	2001	Secondary Education

Work experience:

2007–present	K-Projekt AS	Project manager
2006–2007	AS EG Võrguteenus	Specialist
2005–2006	AS Eesti Gaas	Specialist

Language skills:

Language	Level
Russian	native language
Estonian	higher level
English	average level
German	primary level

Scientific degree Master of Science in Engineering
Certificate of education Tallinn Technical University, 2006
Scientific work Development of Theory of the Dispersed Gas-Solid Particles Flows

ELULOOKIRJELDUS

Eesnimi Igor
Perekonnanimi Krupenski
Sünniaeg ja -koht 23.06.1983, Estonia
Perekonnaseis Vallaline
Kontaktandmed Kadaka pst 169a/a-24, Tallinn, Eesti,
Telefon: +372 58003989;
E-mail: ikrupenski@gmail.com
Töökoht K-Projekt AS,
Ahtri 6a, 10151 Tallinn
Ametikoht Projektijuht

Hariduskäik:

Õppeasutus	Lõpetamise aeg	Haridus
Tallinna Tehnikaülikool	2006	Tehnikateaduste magister
Tallinna Tehnikaülikool	2005	Tehnikateaduste bakalaureus
Tallinna Tõnismäe Reaalkool	2001	Keskharidus

Teenistuskäik:

2007–käesoleva ajani	K-Projekt AS	Projektijuht
2006–2007	AS EG Võrguteenus	Spetsialist
2005–2006	AS Eesti Gaas	Spetsialist

Keelteoskus:

Keel	Tase
Vene	emakeel
Eesti	kõrgtase
Inglise	kesktase
Saksa	algtase

Teaduskraad Tehnikateaduste magister
*Teaduskraadi välja
andnud asutus, aasta* Tallinna Tehnikaülikool, 2006
Teadustöö põhisuunad Disperssete (gaas-tahked osakesed)
vooluste teooria arendamine

**DISSERTATIONS DEFENDED AT
TALLINN UNIVERSITY OF TECHNOLOGY ON
MECHANICAL AND INSTRUMENTAL ENGINEERING**

1. **Jakob Kübarsepp**. Steel-bonded hardmetals. 1992.
2. **Jakub Kõo**. Determination of residual stresses in coatings & coated parts. 1994.
3. **Mart Tamre**. Tribocharacteristics of journal bearings unlocated axis. 1995.
4. **Paul Kallas**. Abrasive erosion of powder materials. 1996.
5. **Jüri Pirso**. Titanium and chromium carbide based cermets. 1996.
6. **Heinrich Reshetnyak**. Hard metals serviceability in sheet metal forming operations. 1996.
7. **Arvi Kruusing**. Magnetic microdevices and their fabrication methods. 1997.
8. **Roberto Carmona Davila**. Some contributions to the quality control in motor car industry. 1999.
9. **Harri Annuka**. Characterization and application of TiC-based iron alloys bonded cermets. 1999.
10. **Irina Hussainova**. Investigation of particle-wall collision and erosion prediction. 1999.
11. **Edi Kulderknup**. Reliability and uncertainty of quality measurement. 2000.
12. **Vitali Podgurski**. Laser ablation and thermal evaporation of thin films and structures. 2001.
13. **Igor Penkov**. Strength investigation of threaded joints under static and dynamic loading. 2001.
14. **Martin Eerme**. Structural modelling of engineering products and realisation of computer-based environment for product development. 2001.
15. **Toivo Tähemaa**. Assurance of synergy and competitive dependability at non-safety-critical mechatronics systems design. 2002.
16. **Jüri Resev**. Virtual differential as torque distribution control unit in automotive propulsion systems. 2002.
17. **Toomas Pihl**. Powder coatings for abrasive wear. 2002.
18. **Sergei Letunovitš**. Tribology of fine-grained cermets. 2003.
19. **Tatyana Karaulova**. Development of the modelling tool for the analysis of the production process and its entities for the SME. 2004.
20. **Grigori Nekrassov**. Development of an intelligent integrated environment for computer. 2004.
21. **Sergei Zimakov**. Novel wear resistant WC-based thermal sprayed coatings. 2004.
22. **Irina Preis**. Fatigue performance and mechanical reliability of cemented carbides. 2004.
23. **Medhat Hussainov**. Effect of solid particles on turbulence of gas in two-phase flows. 2005.

24. **Frid Kaljas**. Synergy-based approach to design of the interdisciplinary systems. 2005.
25. **Dmitri Neshumayev**. Experimental and numerical investigation of combined heat transfer enhancement technique in gas-heated channels. 2005.
26. **Renno Veinthal**. Characterization and modelling of erosion wear of powder composite materials and coatings. 2005.
27. **Sergei Tisler**. Deposition of solid particles from aerosol flow in laminar flat-plate boundary layer. 2006.
28. **Tauno Otto**. Models for monitoring of technological processes and production systems. 2006.
29. **Maksim Antonov**. Assessment of cermets performance in aggressive media. 2006.
30. **Tatjana Barashkova**. Research of the effect of correlation at the measurement of alternating voltage. 2006.
31. **Jaan Kers**. Recycling of composite plastics. 2006.
32. **Raivo Sell**. Model based mechatronic systems modeling methodology in conceptual design stage. 2007.
33. **Hans Rämmal**. Experimental methods for sound propagation studies in automotive duct systems. 2007.
34. **Meelis Pohlak**. Rapid prototyping of sheet metal components with incremental sheet forming technology. 2007.
35. **Priidu Peetsalu**. Microstructural aspects of thermal sprayed WC-Co coatings and Ni-Cr coated steels. 2007.
36. **Lauri Kollo**. Sinter/HIP technology of TiC-based cermets. 2007.
37. **Andrei Dedov**. Assessment of metal condition and remaining life of in-service power plant components operating at high temperature. 2007.
38. **Fjodor Sergejev**. Investigation of the fatigue mechanics aspects of PM hardmetals and cermets. 2007.
39. **Eduard Ševtšenko**. Intelligent decision support system for the network of collaborative SME-s. 2007.
40. **Rünno Lumiste**. Networks and innovation in machinery and electronics industry and enterprises (Estonian case studies). 2008.
41. **Kristo Karjust**. Integrated product development and production technology of large composite plastic products. 2008.
42. **Mart Saarna**. Fatigue characteristics of PM steels. 2008.
43. **Eduard Kimmari**. Exothermically synthesized B₄C-Al composites for dry sliding. 2008.
44. **Indrek Abiline**. Calibration methods of coating thickness gauges. 2008.
45. **Tiit Hindreus**. Synergy-based approach to quality assurance. 2009.

46. **Karl Raba**. Uncertainty focused product improvement models. 2009.
47. **Riho Tarbe**. Abrasive impact wear: tester, wear and grindability studies. 2009.
48. **Kristjan Juhani**. Reactive sintered chromium and titanium carbide- based cermets. 2009.
49. **Nadežda Dementjeva**. Energy planning model analysis and their adaptability for Estonian energy sector. 2009.